AD 268 377

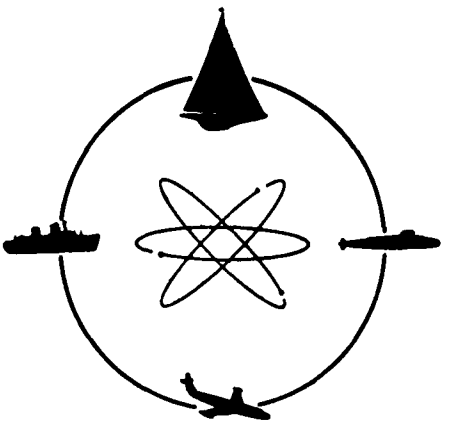

DAVIDSON LABORATORY

PRESSURE FIELD NEAR COUNTERROTATING PROPELLERS

by

S. Tsakonas and J. P. Breslin

September 1961 Report No. 858

PRESSURE FIELD NEAR COUNTERROTATING PROPELLERS

by

S. Tsakonas and J. P. Breslin

Prepared under sponsorship of
Bureau of Ships
Fundamental Hydrodynamics Research Program
Contract Nonr 263(16)
Project S-R009-01-01
Technically Administered by
David Taylor Model Basin

Report No. 858

DAVIDSON LABORATORY
Stevens Institute of Technology
Castle Point Station
Hoboken, New Jersey

ABSTRACT

Expressions for the vibratory pressure field produced by an operating counterrotating propeller system are developed in terms of first and second blade harmonics of the individual propellers. The coefficients of the first and second blade harmonics of a 3-bladed propeller are expressed in closed form in terms of complete elliptic integrals. It is found that the pressure signal due to a counter-rotating propeller can be obtained from the summation of the pressure fields of its two components as though the two propellers operate as separate units, since their mutual interference has been found to contribute little to the total vibratory pressure signal in the near field. This study indicates that the counterrotating propeller system has vibratory characteristics much superior to an equivalent single propeller having the number of blades of one of its components, delivering the same thrust at the same RPM at optimum conditions. A study of the interference effects by means of a two-dimensional analogue indicates that the effect of the forward propeller on the aft is much greater than the effect of the aft propeller on the forward propeller.

INTRODUCTION

Counterrotating propellers are an important means of implementing high-powered propulsive units. It has been generally accepted that, with this propeller system, propulsion losses are minimum and therefore efficiency is high. However, because of mechanical complications this type of propulsion has found little practical application; it has been adopted chiefly for torpedoes. It is the purpose of this investigation to consider the vibration-producing characteristics of counterrotating propellers and to compare them with those of a single propeller with the expectation that counterrotating propellers may show advantages in reducing vibration.

The pressure field generated by an operating propeller is mainly responsible for the vibrations experienced by neighboring boundaries. In view of present technical developments with continuously increasing propulsive forces, the vibratory motions due to the pulsating pressure field may well be expected to increase to a degree which will require either a drastic change in the stern configuration or a different propulsion device. Although other considerations such as avoidance of cavitation and diminution of noise will undoubtedly weigh more heavily in the selection of a new design than the vibration--causing qualities, nevertheless it would appear important in future design work to evaluate these characteristics for the two configurations which are feasible changes from the usual propeller arrangement, viz. counterrotating propellers and shrouded or "nozzle" propellers.

Breslin (1) has made a theoretical study of the pressure field near an operating ship propeller in the open water condition. By using vortex line theory and representing the propeller blade by three types of vorticity, a hub vortex streaming aft along the x-axis, a bound vortex fixed at a position of the blade axis and a tip vortex streaming aft in the form of a helix, he determined the instantaneous pressure at any point in the field.

It was found that the total pressure at a point in the field is

purely convective pressure ($\sim \partial\phi/\partial x$) since the impulsive part of pressure due to the time rate of change of blade position is annulled by part of the convective pressure. It may be stated, therefore, that the pressure can be investigated as a steady-state phenomenon depending on the blade position. This fact makes for considerable simplification in the present investigation. In References 2 and 3, the blade frequency pressure and velocity fields around a marine propeller due to loading and thickness effects have been determined in closed form in terms of complete elliptic integrals. If the mutual interference of the two propellers is neglected and the results of References 2 and 3 are used, the pressure field around two counterrotating propellers will be determined as a function of blade position. In contrast to the case of a single propeller where only the m-blade frequency need be considered, in the case of two counterrotating m-bladed propellers both the m and the 2m blade frequencies ($\frac{m\omega}{2\pi}$ and $\frac{m\omega}{\pi}$) are of practical significance.

In the first part of the present investigation expressions for the fluctuating pressure signal due to the counterrotating propellers have been developed as though the two propellers operate as separate units without any interference between them. Expressions for the first and second blade harmonics of the pressure signal have been evolved for the case of a pair of 3-bladed propellers in terms of complete elliptic integrals.

The second part of this investigation is concerned with the mutual interference of blades as they approach and pass each other. The interference leads to a time-dependent increment of lift (thrust) which averaged over time remains close to zero but instantaneously may be large although of short duration. This interference effect is studied under two-dimensional flow conditions which are more amenable to mathematical analysis than the three-dimensional flow. The magnitude of the interference effect on the pressure in an actual three-dimensional case will be much smaller.

The third part deals with the evaluation of the pressure field in the presence of 3-0-3 counterrotating propellers. (The first digit in the designation denotes the number of blades in the forward component, the second the number of countervanes and the third the number of blades

in the after component.) The expressions evolved in the analysis are used to determine the coefficients of the 3rd and 6th harmonics of the pressure signal due to each 3-bladed propeller separately at 6 different stations, up to an axial distance of 0.8 of the propeller radius, for four different tip clearances. By combining the corresponding Fourier coefficients the pressure signal in the field of the 3-0-3 propeller system is determined. In addition, the case of a single 3-bladed propeller producing equivalent thrust and having the same RPM as the 3-0-3 system is treated and its pressure field compared with that of the counterrotating propellers.

This study is prepared under Contract Nonr 263(16), of the Bureau of Ships Fundamental Hydrodynamics Research Program, Project S-R009-01-01, and technically administered by the David Taylor Model Basin.

ANALYSIS

Part I

Simplified Theory for the Oscillatory Pressure Field About Counterrotating Propellers

In this propeller system two coaxial propellers are situated a short distance apart and are rotated in opposite directions. Due to the short axial separation there will be mutual interference between the two propellers. In this part of the investigation, however, the blade interference effects will be neglected and the pressure field will be evaluated as if the two propellers influenced the field separately.

Breslin (1) has shown by vortex line theory and also by use of doublet distributions that the linearized pressure charge in an otherwise unbounded fluid due to an operating m-bladed propeller is the sum of thrust-produced pressure and torque-produced pressure as follows:

$$\frac{P}{T'} = \frac{P_T + P_Q}{T'}$$

where

$$\frac{P_T}{T'} = -\frac{x}{2m}\int_o^1 \frac{s\ ds}{R_o^3} \tag{1}$$

and

$$\frac{P_Q}{T'} = -\frac{J}{2\pi m}\int_o^1 \frac{r \sin\alpha\ ds}{R_o^3} \tag{2}$$

T' = thrust loading coefficient = $T/\pi b^2$ where T is thrust and b propeller radius

m = number of blades

$J = \frac{v}{nD}$ = advance ratio, where v is the velocity of advance

n = r.p.s. and D = propeller diameter

$R_o = (x^2+r^2+s^2- 2rs\cos\alpha)^{1/2}$

x, r, γ = cylindrical coordinates of the field point in the fluid at which the pressure signal is calculated.

$\alpha = \theta - \gamma$, where θ is the blade position angle.

s is dimensionless blade span.

The foregoing expressions (1) and (2) are referred to a coordinate system with the origin at the propeller center (Fig. 1) and all the linear dimensions are multiples of the propeller radius b .

In the counterrotating propeller configuration, the origin of the coordinate system is taken on the axis of rotation midway between the propeller mid-planes, i.e. at a distance $\pm x_o$ from the forward and aft propeller, respectively. The x-axis is taken along the axis of rotation opposite in direction to the main stream flow (Fig. 2).

Since Eqs. 1 and 2 have been developed by making use of the results of the linearized theory, the instantaneous pressure signal of the counterrotating propeller configuration will be given by

$$P = (P_T^{(1)} + P_Q^{(1)}) + (P_T^{(2)} + P_Q^{(2)}) \quad . \tag{3}$$

where the forward and the after propeller are designated by superscript 1 and 2, respectively, and $P_T^{1,2}$ and $P_Q^{1,2}$ are as given in Eqs. (1) and (2) with the only difference that x should be replaced by $x - x_o$ for the forward propeller and by $x + x_o$ for the after propeller.

An important aspect of the pressure field is revealed by seeking the contribution at m and $2m$ frequencies. The total pressure signal at any given point of the field will be expressed in terms of Fourier coefficients as

$$\frac{P}{T'} = \sum_{i=1}^{i=2}\left\{ \sum_{k=0}^{\infty} A_k^i \cos k\alpha^i + \sum_{n=1}^{m-1}\sum_{k=0}^{\infty} A_k^i \cos k\left(\alpha^i + \frac{2\pi}{m} n\right)\right\} +$$

$$\sum_{i=1}^{i=2}\left\{\sum_{k=0}^{\infty} B_k^i \sin k\,\alpha^i + \sum_{n=1}^{m-1}\sum_{k=0}^{\infty} B_k^i \sin k\,(\alpha^i + \frac{2\pi}{m} n)\right\} \qquad (4)$$

where $\alpha^i = \theta^i - \gamma$ = the instantaneous angular position of the blade relative to the station where the pressure signal is determined. In the first summation over i, 1 and 2 correspond to the forward and aft propeller. The second summation over k gives the contribution of all harmonics and the third summation from $n = 1$ to $m - 1$ arises through the inclusion of the contributions of the other $m - 1$ blades which are spaced at angular intervals of $\frac{2\pi}{m}$, $\frac{4\pi}{m}$ etc.

It is shown in Appendix A that

$$\sum_{n=1}^{n=m-1} \cos k(\alpha^i + \frac{2\pi}{m} n) = \begin{cases} -\cos k\alpha^i & \text{for } k \text{ not an integer multiple of } m. \\ (m-1)\cos k\,\alpha^i & \text{for } k \text{ an integer multiple of } m. \end{cases}$$

and

$$\sum_{n=1}^{n=m-1} \sin k(\alpha^i + \frac{2\pi}{m} n) = \begin{cases} -\sin k\,\alpha^i & \text{for } k \text{ not an integer multiple of } m. \\ (m-1)\sin k\,\alpha^i & \text{for } k \text{ an integer multiple of } m. \end{cases}$$

For the case of k a non-integer multiple of m, $P = 0$ so that there is no contribution to the pressure signal from the harmonics which are not integer multiples of the blade frequencies. The only terms which contribute to the pressure signal are harmonics of $m\,\alpha_1$ or higher multiples of $m\,\alpha$, which are known as the harmonics of

the blade frequencies. Therefore, the total pressure signal will be given as

$$m\frac{P}{T'} = m\sum_{i=1}^{i=2}\sum_{n=1}^{\infty} A_{nm}^{i}\cos nm\,\alpha^{i} + m\sum_{i=1}^{i=2}\sum_{n=1}^{\infty} B_{nm}^{i}\sin nm\,\alpha^{i} \qquad (5)$$

When only the first two blade frequencies are considered,

$$\frac{P}{T'} = \frac{P^{(1)}+P^{(2)}}{T'} = A_m^{(1)}\cos m\alpha^{(1)} + A_m^{(2)}\cos m\alpha^{(2)} + B_m^{(1)}\sin m\alpha^{(1)} + B_m^{(2)}\sin m\alpha^{(2)}$$
$$+ A_{2m}^{(1)}\cos 2m\alpha^{(1)} + A_{2m}^{(2)}\cos 2m\,\alpha^{(2)} + B_{2m}^{(1)}\sin 2m\alpha^{(1)} + B_{2m}^{(2)}\sin 2m\,\alpha^{(2)} \qquad (6)$$

The angular blade positions $\alpha^{(1)}$ and $\alpha^{(2)}$ for the two components of the counterrotating configuration change with time according to the relationship

$$\frac{d\alpha^{(1)}}{dt} - \frac{d\alpha^{(2)}}{dt} = 2\omega$$

since both are rotating with the same angular velocity ω around the same axis but in opposite directions. Then the angular blade position of the after propeller is given in terms of the forward by

$$\alpha^{(2)} = \alpha^{(1)} - 2\omega t + c$$

where c is a constant depending on the initial conditions. Under the assumption that at $t = 0$, $\alpha^{(1)} = 0$ and $\alpha^{(2)} = \frac{2\pi}{m}$, the above relation becomes

$$\alpha^{(2)} = \alpha^{(1)} - 2\omega t + \frac{2\pi}{m}$$

It is of interest to examine the situation at two instants of time, when the blades are in alignment (in phase) and when they are farthest from alignment (out-of-phase). The in-phase condition will

exist when

$$\alpha^{(1)} = \alpha^{(2)} \quad \text{or} \quad t = \frac{\pi}{m\omega} \tag{7}$$

and the out-of-phase condition will be given when

$$\alpha^{(2)} = \alpha^{(1)} + \frac{\pi}{m} \quad \text{or} \quad t = \frac{\pi}{2m\omega} \tag{8}$$

i.e. when the blades of the after propeller bisect the angles between the blades of the forward propeller. For the in-phase condition, the total pressure signal will be given (see Appendix B) by

$$\frac{P}{T'} = (A_m^{(1)} + A_m^{(2)})\cos m\alpha^{(1)} + (A_{2m}^{(1)} + A_{2m}^{(2)})\cos 2m\alpha^{(1)}$$

$$+ (B_m^{(1)} + B_m^{(2)})\sin m\alpha^{(1)} + (B_{2m}^{(1)} + B_{2m}^{(2)})\sin 2m\alpha^{(1)} \tag{9}$$

where A_m^i, A_{2m}^i, B_m^i and B_{2m}^i are the m and $2m$ harmonics of the Fourier series representing the expressions for the pressure components of Eq.(2). For the out-of-phase case, the total pressure signal will be given (see Appendix B) by

$$\frac{P}{T'} = (A_m^{(1)} - A_m^{(2)})\cos m\alpha^{(1)} + (A_{2m}^{(1)} + A_{2m}^{(2)})\cos 2m\alpha^{(1)}$$

$$(B_m^{(1)} - B_m^{(2)})\sin m\alpha^{(1)} + (B_{2m}^{(1)} + B_{2m}^{(2)})\sin 2m\alpha^{(1)} \tag{10}$$

Therefore for all instants at which the blades are in coincidence the pressure signal contains m-blade frequencies as well as 2m-blade frequencies, whereas out-of-phase it seems that the m-blade signals tend to cancel each other leaving mainly the 2m-frequencies. As will be seen later on from the calculations, the cancellation will occur at large distance from the propeller plane.

In order to calculate the pressure signal at any point in the

field by means of eq. (9) and (10) it is necessary to evaluate the Fourier coefficients for the first and second blade frequencies in advance. This can be done by restricting our attention to the pressure field near a single m-bladed propeller. Then the general expressions which have been developed may easily be transformed to equivalent expressions for the description of the pressure field due to a pair of counterrotating propellers at a distance $\pm x_o$ from the new origin (Fig. 2).

As demonstrated in Reference 2, for the case of 3-bladed propellers the thrust contribution contains only cosine terms and the torque contribution only sine terms. It was found in that reference that the Fourier coefficients of the first blade harmonic of the pressure signal due to the loading are given by

$$A_3 = - c_2 \frac{x}{\pi} cr \left\{ I_a\left[r+1+ \frac{5}{n}(r+1)+ \frac{4}{n^2}(r+1)\right]- I_b\left[2r+ \frac{10r}{n} + \frac{8}{n^2} r\right] \right.$$

$$\left. - A_o\left[\frac{4r+5}{n} - \frac{4(r+1)}{n^2}\right]+ A_2\left[\frac{8r+16}{n} + \frac{8r}{n^2}\right]- A_4\left[\frac{16}{n}\right] \right\} \qquad (11)$$

for the cosine term and

$$B_3 = c_1 \frac{4r}{\pi} c \left\{ \frac{I_a}{4n}\left[3r+3+ \frac{4r+4}{n}\right]- \frac{I_b}{2n}\left[3r+ \frac{4r}{n}\right] \right.$$

$$- \frac{A_o}{4n}\left[3r+3+ \frac{4r+4}{n}\right]+ \frac{A_2}{4n}\left[22r+16+ \frac{8r}{n}\right]$$

$$\left. - \frac{A_4}{4n}[48r+16]+ \frac{A_6}{4n}[32r] \right\} \qquad (12)$$

for the sine coefficient, where

$$c = \frac{4}{(1+x^2+r^2)^{1/2}(1+k^2)^{1/2}x^2}$$

$c_1 = \frac{J}{2\pi}$ (the coefficient of the torque component)

$c_2 = \frac{1}{2}$ (the coefficient of the thrust component)

$$n = \frac{r^2}{x^2} \quad , \quad k^2 = \frac{2r}{1+x^2+r^2} \quad , \quad k'^2 = \frac{2k^2}{1+k^2}$$

$$I_a = \frac{\alpha^2}{\alpha^2-\beta^2}\prod(\alpha^2,k') - \frac{\beta^2}{\alpha^2-\beta^2}\prod(\beta^2,k')$$

$$I_b = \frac{1}{\alpha^2-\beta^2}\prod(\alpha^2,k') - \frac{1}{\alpha^2-\beta^2}\prod(\alpha^2,k')$$

$$A_o = F(k') \qquad A_2 = \frac{1}{(k')^2}\,[(F(k') - E(k')] \tag{13}$$

$$A_{2m+2} = \frac{2m(1+k'^2)A_{2m} + (1-2m)A_{2m-2}}{(2m+1)(k')^2} \quad (m \text{ integer})$$

$\prod(\alpha^2,k')$, $\prod(\beta^2,k')$ are complete elliptic integrals of the third kind

$F(k')$ and $E(k')$ are complete elliptic integrals of the first and second kind respectively

$$\left\{\begin{matrix}\alpha^2 \\ \beta^2\end{matrix}\right\} = 2[-n \pm \sqrt{n^2+n}]$$

and other symbols are as defined in eq. (2).

In Appendix C, the general procedure for determining the coefficients of the second blade frequencies of the pressure signal due to a 3-bladed propeller and the evaluation of some representative integrals are demonstrated. The results are:
for the cosine coefficient,

$$A_6 = 2c_2\left\{ -32\left(1+\frac{1}{n}\right)^3 + 48\left(1+\frac{1}{n}\right)^2 - 18\left(1+\frac{1}{n}\right) + 1 + 32\left(\frac{1}{n}\right)^{1/2}\left(1+\frac{1}{n}\right)^{5/2} - 32\left(\frac{1}{n}\right)\left(1+\frac{1}{n}\right)^{3/2} \right.$$

$$\left. + 6\left(\frac{1}{n}\right)^{1/2}\left(1+\frac{1}{n}\right)^{1/4} \right\} +$$

$$+ \frac{x\lambda c_2}{\pi}\left\{ - I_a\left[n\left(1+\frac{1}{n}\right) + \left(19+\frac{18}{r}\right) + \frac{1}{n}\left(66+\frac{48}{r}\right) + \frac{1}{n^2}\left(80+\frac{32}{r}\right) + \frac{32}{n^3}\right] \right.$$

$$+ 2I_b\left[\frac{1}{r}(n+18) + \frac{16}{rn}\left(3+\frac{2}{n}\right)\right] + 2A_o\left[\left(9+\frac{9}{r}\right) + \frac{1}{n}\left(33+\frac{24}{r}\right) + \frac{1}{n^2}\left(40+\frac{16}{r}\right) + \frac{16}{n^3}\right]$$

$$-4A_2\left[48+\frac{57}{r}\right) + \frac{1}{n}\left(80+\frac{56}{r}\right) + \frac{1}{n^2}\left(32+\frac{16}{r}\right)\right]$$

$$+64A_4\left[\left(11+\frac{17}{r}\right) + \frac{1}{n}\left(13+\frac{6}{r}\right) + \frac{2}{n^2}\right] - 128\,A_6\left[\left(8+\frac{19}{r}\right) + \frac{1}{n}\left(8+\frac{2}{r}\right)\right]$$

$$\left. +512\,A_8\left[1+\frac{5}{r}+\frac{1}{n}\right] - 1024\,A_{10}\left[\frac{1}{r}\right] \right\} \qquad (14)$$

where $\lambda = \dfrac{4}{(1+x^2+r^2)^{1/2}(1+k^2)^{1/2}}$

and for the corresponding sine coefficient,

$$B_6 = \frac{2c_1}{r}\left\{ 32\,n^{1/2}\left(1+\frac{1}{n}\right)^3 - 64\,n^{1/2}\left(1+\frac{1}{n}\right)^2 + 38\,n^{1/2}\left(1+\frac{1}{n}\right) - 6\,n^{1/2} - \right.$$

$$\left. - 32\left(1+\frac{1}{n}\right)^{5/2} + 48\left(1+\frac{1}{n}\right)^{3/2} - 18\left(1+\frac{1}{n}\right)^{1/2} + \frac{1}{\left(1+\frac{1}{n}\right)^{1/2}} \right\} +$$

$$+ \frac{c_1 cr}{n}\left\{ - I_a\left[\frac{6r+6}{n} + \frac{38r+32}{n^2} + \frac{64r+32}{n^3} + \frac{32r}{n^4}\right] + I_b\left[\frac{12}{n} + \frac{64}{n^2} + \frac{64}{n^3}\right] \right.$$

$$\left. + A_o\left[\frac{6r+6}{n} + \frac{38r+32}{n^2} + \frac{64r+32}{n^3} + \frac{32r}{n^4}\right] \right.$$

$$- A_2\left[\frac{152r+140}{n} + \frac{256r+192}{n^2} + \frac{128r+64}{n^3}\right] \qquad (15)$$

$$+ A_4\left[\frac{1176r+896}{n} + \frac{768r+384}{n^2} + \frac{128r}{n^3}\right]$$

$$-A_6\left[\frac{4096r+2304}{n} + \frac{1024r+256}{n^2}\right]$$

$$+A_8\left[\frac{7168r+2560}{n} + \frac{512r}{n^2}\right]$$

$$-A_{10}\left[\frac{6144r+1024}{n}\right] + A_{12}\left[\frac{2048r}{n}\right]\Bigg\}$$

Expressions (11) (12) (14) and (15) have been used together with eqs. (9) and (10) to evaluate the pressure signal of the 3-0-3 counter-rotating propeller configuration. At $x = 0$, these expressions show signs of indeterminacy but after straight-forward manipulation in conjunction with a limiting procedure they are reduced to:

$$A_3 = 0 \qquad A_6 = 0$$

$$B_3 = \frac{4r}{\pi} c_1 c' \left\{ - 3A_o(r+1)+2(11r+8)A_2-16(32r+1)A_4+32rA_6 \right\} \qquad (16)$$

$$B_6 = \frac{c_1 c'}{\pi} \Big\{ A_o(6r+6)-A_2(152r+140)+A_4(1176r+896)$$
$$-A_6(4096r+2304)+A_8(7168r+2560)$$
$$-A_{10}(6144r+1024)+A_{12}(2048r) \Big\}$$

where $c' = \dfrac{1}{r^2(1+r^2)^{1/2}(1+k^2)^{1/2}}$

In spite of the fact that closed-form expressions have been developed for the fluctuating pressure signal near the counterrotating propeller, the numerical method described in Reference 4 is used in the

present work since a coding program for the evaluation of the total instantaneous pressure signal was available for the ELECOM 100 computer.

Hence, as in Reference 4, the total oscillatory pressure "signature" for a single blade is plotted for the angular interval $-\pi$ to π . Since the pressure equation is linear the contribution of individual blades can be superimposed and the result for three blades, for example, can be obtained from that for a single blade by summing the contributions of the one blade at three 120° intervals. The resulting composite curve which has a cycle of 120° for three blades, can be analyzed harmonically by a 24-ordinate numerical procedure.

Part II

Approximate Evaluation of Pressure Fluctuation Arising from the Blade Interference Effects

In the previous section the vibratory pressure field arising from the m-0-m counterrotating propeller system has been evaluated as if the two propellers operate separately. It is known, however, that because of the small axial distance between the two propellers their mutual interference will develop a pressure field which will give rise to a time-dependent lift. It is believed that as two blade sections approach and pass each other in relative motion this time-dependent lift remains on the average very close to zero, but instantaneously it may be large although of short duration. The interaction phenomenon can possibly produce strong fluctuations in the close proximity of the propellers and therefore it should be included in the analysis of the oscillatory pressure field of counterrotating propellers. A study of this interference phenomenon as a three-dimensional unsteady flow problem is mathematically untractable. It has been decided therefore to study this phenomenon as a two-dimensional problem with the thought that if such contributions to the pressure can be shown to be small then they can be safely assumed as small in the actual three-dimensional case. It is known that in the three-dimensional mathematical model (with finite span), which is described by a bound vortex line and free vortex shed from the tips of the wing, the induced velocity field is of smaller amplitude than is that of the corresponding two-dimensional model with infinite span represented by a lifting line. The trailing vortex reduces the angle of attack of the incoming flow, and consequently the lift and the generated pressure will be diminished.

The two-dimensional problem that is perhaps most closely related to the one posed by the motion of the propeller blades is that presented by two arrays of finite-chord foil sections moving with the same angular velocity Ω but in opposite directions as shown in Fig. 2b. It is, however, more convenient to study these effects as of the relative motion of one cascade with respect to the other.

If the string of blades of the forward propeller is assumed to be fixed in space the cascade of the after propeller blades will then be moving with angular velocity 2Ω. This sort of blade arrangement is identical with that encountered in the stator and rotor cascades of axial-flow machinery.

In order to preserve as many as possible of the geometric and kinematic characteristics of the three-dimensional problem in this two-dimensional model, so that the latter will become a reasonably useful analogue, it will be assumed that the geometric blade characteristics are those existing at the effective radius $b_e = 0.7b$ of the propeller. The blade spacing d will be determined as

$$d_{s,r} = \frac{2\pi (b_e)_{s,r}}{m_{s,r}}$$

where m is the number of blades in the propeller and subscripts s and r refer to the stator and rotor respectively. The incoming flow to this cascade arrangement has a velocity V in the axial direction equivalent to the speed of advance and a tangential velocity equal to the product of effective radius and angular velocity.

This two-dimensional analogue has been studied in Reference 5 as a useful model for evaluation of the induced effects on the blades of a typical turbomachine moving through a nonuniform field disturbed by the stationary blades. The results of the theory of a single thin airfoil in non-uniform motion have been utilized in order to calculate the resulting unsteady effects on an infinite cascade of blades moving with respect to a stationary row of blades (stator). Expressions have been developed for the induced velocities and the lift on a single rotor blade due to the steady-state circulation distribution of each and every stator blade as well as to the effect of the vorticities shed by the stator blades and for the lift on a single stator blade due to the steady-state circulation distribution of each rotor blade. Both flat plate and elliptic distributions of the steady circulation are assumed in Reference 5.

One must keep in mind, however, that in reality the stator-

rotor interference problem is much more complicated and many more factors are involved than are treated in the above reference. Each foil is influenced by 1) its own wake, 2) the variable bound vortices of the fellow members of its own blade row, 3) their wakes, 4) the variable bound vortices of members of the other blade row, 5) their wakes and finally 6) by the displacement effects of the blades, since each blade is of finite chord and thickness. The problem can be rigorously treated by solving a pair of integral equations which state the requirement of the boundary conditions on the stationary and moving blades, viz. the tangency of the flow along the moving blades and zero velocity across the stationary blades. The solution of this system of integral equations will determine the circulation distribution (loading) of each blade and the corresponding pressure field generated by the mutual interference of the blades will thus be obtained.

In Reference 5 Kemp and Sears have shown that the velocity, $v^{r}{}_{1}$, induced at a rotor blade by the motion of the steady stator circulation ${}_{o}\Gamma^{s}$ is given by

$$v^{r}{}_{1}(x_r,t) = - {}_{o}\Gamma^{s} \frac{e^{i\alpha_r}}{2d_s} + \frac{{}_{o}\Gamma^{s}}{2\pi c_r} \sum_{m} G_m^{r} \exp\left(- \frac{2\pi m}{d_s} e^{i\alpha_r} x_r\right) e^{i\nu_r m t} \qquad (17)$$

where

$$G_m^{r} = - \frac{\pi\sigma_r d_r}{d_s} e^{i\alpha_r} H_m^{s} \exp\left\{ - \frac{\pi m \sigma_r d_r}{d_s} \left[\frac{b_p}{c_r}\left(1 + i \tan\alpha_r - \frac{iU}{V_s \cos\alpha_s}\right) - \frac{iU}{V_r}\right]\right\}$$

$$H_m^s = \begin{cases} J_o(m\lambda_s) + iJ_1(m\lambda_s) & \text{for the case of a flat-plate distribution} \\ -\dfrac{2ie^{ia_s}}{\pi\sigma_s m} J_1(m\lambda_s) & \text{for the case of an elliptic circulation distribution} \end{cases}$$

σ = solidity of row, $\sigma_r = \dfrac{2c_r}{d_r}$ and $\sigma_s = \dfrac{2c_s}{d_s}$, solidity of rotor and stator, respectively.

$\lambda_s = \pi\sigma_s e^{+i(\pi/2 - a_s)}$

ν_r = circular frequency of motion = $\dfrac{2\pi U}{d_s}$

b_p = axial distance between the propeller planes

a = angle of blade stagger (the complement of the effective pitch angle)

U = rotational speed of rotor, positive down

$V_{r,s}$ = inflow speed relative to blade

J_o, J_1 = Bessel function of zero and first order, respectively.

x, y = Cartesian coordinates of point in space referred to a system of axes fixed in the blade with the origin at the center (see Figure 2b) and with positive x in the direction of the trailing edge.

As mentioned before, the additional effects on the rotor blades of the vortex wake shed by the stator blades are also taken into account in the above reference. In this case the induced velocity v^{r_2} (r_2 indicates the effect of wake vorticity) at the rotor blades is given in complex Fourier series form by:

$$v^{r_2} = \sum_m \sum_k{}' v_{mk} \exp\left[i\nu_r k(t - x_r/V_r)\right] \tag{18}$$

where

$$v_{mk} = -\frac{{}^{o}\Gamma^{r}}{d_s \cos a_s} \exp\left[-im\pi\sigma_r \left(\frac{b_p U}{V_s c_r \cos a_s} + \frac{U}{V_r}\right) + i\omega_r k\right] \left\{ F_m^s \frac{\left(\frac{V_s d_r}{V_r d_s}\right)\frac{k}{m}}{1 + \cot^2\beta\left[1 - \frac{V_s d_r}{V_r d_s}\frac{k}{m}\sec\beta\right]^2} \right\}$$

$\omega_r = \nu_r c_r / V_r$ = reduced frequency

$$F_m^s = G_m^s \left[J_o(\lambda_s m) - i\, J_1(\lambda_s m)\right]$$

$$G_m^s = \frac{\pi\sigma_s d_s}{d_r} e^{-i\alpha_s} H_m^r \exp\left\{-\pi m\sigma_r\left[\frac{b_p}{c_r}\left(1 + i\tan\alpha_r - \frac{iU}{V_s\cos\alpha_s}\right) - \frac{iU}{V_r}\right]\right\}$$

$$H_m^r = \begin{cases} J_o(m\lambda_r) + iJ_1(m\lambda_r) & \text{for a flat plate circulation distribution} \\ \dfrac{2ie^{-i\alpha_r}}{\pi\sigma_r m} J_1(m\lambda_r) & \text{for an elliptic circulation distribution} \end{cases}$$

and $\lambda_r = \pi\sigma_r e^{-i(\pi/2-\alpha_r)}$

$\sum_m$ = summation over the number of blades. Theoretically m varies from one to infinity, however only a few terms of the series contribute to the induced velocity v_{r_2}

$\sum_k'$ = summation over k from $-\infty$ to ∞ omitting $k = 0$. This summation actually indicates that the vortex wake shed by the stator is made up of the superposition of waves of all harmonics from $-\infty$ to $+\infty$.

Finally the expression of the velocity v^s at the stator blade induced by the motion of the steady rotor circulation ${}_o\Gamma^r$ is given in Reference 5 as

$$v^s(x_s,t) = \frac{{}_o\Gamma^r e^{-i\alpha_s}}{2d_r} + \frac{{}_o\Gamma^r}{2\pi c_s} \sum_m G_m^s \exp\left(\frac{2\pi m}{d_r} e^{-i\alpha_s} x_s\right) e^{i\nu_s mt} \qquad (19)$$

where x_s is referred to a system of axes fixed in the stator blade positive toward the trailing edge, $\nu_s = 2\pi U/d_r$ and the other symbols are as defined previously.

The foregoing expressions for the induced velocities at the rotor blades and stator blades can be written in a more convenient form by replacing the exponentials with well-known series. For instance, the exponent which appears in eq. (17) can be written as

$$\frac{2\pi m}{d_s} x_r e^{i\alpha_r} = i\,(2\pi m \frac{c_r}{d_s}) \frac{x_r}{c_r} e^{-i(\pi/2 - \alpha_r)}$$

$$= i\,\mu_{r_1}^{m} \frac{x_r}{c_r}$$

where $\mu_{r_1}^{m} = \frac{2\pi m c_r}{d_s} e^{-i(\pi/2 - \alpha_r)}$ (20)

With the transformation

$$x_r = c_r \cos\theta$$

the corresponding exponential is written as

$$\exp\left(-\frac{2\pi m}{d_s} e^{i\alpha_r} x_r\right) = e^{-i\mu_{r_1}^{m}\cos\theta} = J_o(\mu_{r_1}^{m}) + 2 \sum_{n=1}^{\infty} (-i)^n J_n(\mu_{r_1}^{m}) \cos n\theta$$

Therefore, the unsteady induced velocity on a rotor blade due to the steady state circulation, i.e. eq. (17) restricted to the time-dependent term alone, will be given by

$$v^{r_1} = \frac{\Gamma_o^s}{2\pi c_r} \sum_m G_m^r e^{i\nu_r m t} \left\{ J_o(\mu_{r_1}^{m}) + 2 \sum_{n=1}^{\infty} (-i)^n J_n(\mu_{r_1}^{m}) \cos n\theta \right\} \quad (21)$$

where all symbols are as defined in eq. (17) and eq. (20).

In a similar fashion the unsteady induced velocity at a rotor blade due to the vortex wake shed by the stator blades (see eq. 18) and the velocity on the stator blade induced by the motion of the steady rotor circulation will be given by

$$v^{r_2} = \sum_m \sum_k{}' v_{mk} e^{i\nu_r k t} \left[J_o(\mu_{r_2}^{k}) + 2 \sum_{n=1}^{\infty} (-i)^n J_n(\mu_{r_2}^{k}) \cos n\theta \right] \quad (22)$$

and

$$v = \frac{{}^{s}\Gamma_{o}^{r}}{2\pi c_s} \sum_{m} {}^{s}G_{m}^{m} e^{i\nu_s mt} [J_o(\mu_s) + 2 \sum_{n=1}^{\infty} (-i)^n J_n(\mu_s) \cos n\theta] \qquad (23)$$

respectively, where

$$\mu_{r_2}^{k} = \frac{2\pi k U c_r}{V_r d_s} \qquad (24)$$

$$\mu_s^m = \frac{2\pi m c_s}{d_r} e^{-i(\pi/2+\alpha_s)}$$

In References 6 and 7 the acceleration potential of a thin airfoil oscillating with an arbitrary mode or with an arbitrary velocity distribution has been derived in the ζ-plane, in which plane a line segment of the physical z-plane, from $x = -1$ to $x = 1$, has been transformed into a circle of unit radius as shown in Sketch 1.

For an airfoil with an arbitrary velocity distribution

$$v(x,\theta) = W e^{i\omega t} (P_o + 2 \sum (-1)^n P_n) \qquad (25)$$

the corresponding acceleration potential is given by

$$\phi = 2UW[C(k)(P_o+P_1)-P_1] \frac{\sin\theta_1}{r_1} + 2UW \sum_{n=1} \left(\frac{ik}{2n} P_{n-1} + P_n - \frac{ik}{2n} P_{n+1}\right) \frac{\sin n\theta}{r^n} \qquad (26)$$

where $C(k)$ = Theodorsen's function of argument k

$$= \frac{K_1(ik)}{K_1(ik)+K_o(ik)}$$

$K_1(ik)$ and $K_o(ik)$ = Modified Bessel functions of the second kind of order 1 and zero, respectively

k = reduced frequency

U = velocity of incoming flow in the direction of the airfoil chord.

r_1, θ_1 = polar coordinates of the field point from the leading edge. (see Sketch 1)

r, θ = polar coordinates of the field point from the center of the airfoil. (see Sketch 1)

(It must be noted that all linear dimensions in the above formulas are expressed in terms of the semi-chord c of the foil.)

By the definition of the acceleration potential the pressure signal at any point in the ζ-plane will be given by

$$P = -\rho\phi \qquad (27)$$

and the lift distribution on the foil will be obtained from eq. (27) by putting $r=1$, $r_1=2\cos\theta_1$ in eq. (26). Now if eq. (25) is compared with the equations for the induced velocities on rotor or stator, it is easy to identify the corresponding terms in each case. For the case of flow (r_1) of the steady stator circulation past the rotor, the various terms can be identified as follows:

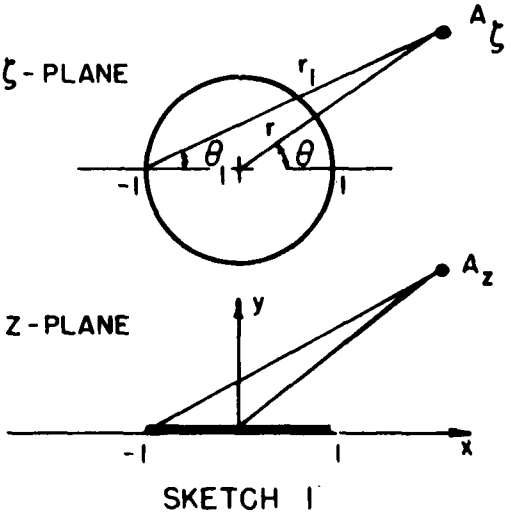

SKETCH 1

$$k = \mu^m_{r_1}$$

$$P_o = J_o(\mu^m_{r_1}) \quad \text{and} \quad P_n = (-i)^n J_n$$

It is easy to show that

$$\frac{ik}{2n} P_{n-1} + P_n - \frac{ik}{2n} P_{n+1} = \frac{ik}{2n} (-i)^{n-1} J_{n-1} + (-i)^n J_n - \frac{ik}{2n} (-i)^{n+1} J_{n+1}$$

$$= 0 \quad \text{for all} \quad n \geq 1$$

Hence the corresponding acceleration potential in the ζ-plane will be given by

$$\phi_{r_1} = \frac{\rho \Gamma^s V_r}{\pi c_r} \frac{\sin\theta_1}{r_1} \sum_{m=1} G_m^r e^{i\nu_r mt} \left\{ C(\mu_{r_1}^m)[J_o(\mu_{r_1}^m) - i J_1(\mu_{r_1}^m)] + iJ_1(\mu_{r_1}^m) \right\}$$

The unsteady pressure signal in non-dimensional form P_{r_1}/T' at a point with polar coordinates r_1, θ_1 in the ζ-plane will be given by

$$\frac{P_{r_1}}{T'} = -\left(\frac{2V_r}{m\Omega c_r}\right) \frac{\sin\theta_1}{r_1} \sum_{m=1} G_m^r \left\{ C(\mu_{r_1}^m)[J_o(\mu_{r_1}^m) - i J_1(\mu_{r_1}^m)] + iJ_1(\mu_{r_1}^m) \right\} \qquad (28)$$

where the propeller disc loading coefficient

$$T' = \frac{T}{\pi b^2} = \frac{m\rho\Omega_o \Gamma^s}{2\pi}$$

has been used. In a similar fashion the pressure signals due to flow (r_2), which concerns the effects of the stator wakes on the rotor, and to flow (s) of steady rotor circulation on the stator will be given by the following forms, respectively

$$\frac{P_{r_2}}{T'} = \left(\frac{4\pi V_r}{m\Omega d_s \cos\alpha_s}\right) \frac{\sin\theta_1}{r_1} \sum_{m=1}^{\infty} \sum_{k=-\infty}^{\infty}{}' v_{mk} \left\{ C(\mu_{r_2}^k)[J_o(\mu_{r_2}^k) - iJ_1(\mu_{r_2}^k)] + iJ_1(\mu_{r_2}^k) \right\} \qquad (29)$$

and

$$\frac{P_s}{T'} = -\left(\frac{2V_s}{m\Omega c_s}\right) \frac{\sin\theta_1}{r_1} \sum_{m} G_m^s \left\{ C(\mu_s^m)[J_o(\mu_s^m) - iJ_1(\mu_s^m)] + i J_1(\mu_s^m) \right\} \qquad (30)$$

where all the linear dimensions outside the first parenthesis are expressed as fractions of the semi-chord at 0.7b. It must be kept in mind that P_r and P_s are referred to coordinate systems fixed at rotor and stator foils respectively. The function $\sin\theta_1/r_1$ is determined for points of known polar coordinates in the ζ-plane of each foil. It can be generally stated that the function $\sin\theta_1/r_1$ is the field point function

which depends also on the geometric characteristics of the propeller and the remaining terms constitute the loading function.

For computational simplification it will be assumed that at time $t = 0$ the center of the chord of stator or rotor lies on the x-axis of the coordinate system fixed relative to ship and the counter-rotating propeller. Then by a simple trigonometric transformation a point with coordinates x_o, y_o in the original system will be determined with respect to the orthogonal axes fixed in the rotor or stator blades as follows:

For instance for the case when the origin of the blade axes is on the x-axis of the ship the coordinates of a point (x_o, y_o) will be

$$x_r = (x_o - b_p/2)\cos\alpha_r + y_o \sin\alpha_r$$

$$y_r = -(x_o - b_p/2)\sin\alpha_r + y_o \cos\alpha_r$$

with respect to a system fixed in the rotor, and

$$x_s = (x_o + b_p/2)\cos\alpha_s - y_o \sin\alpha_s$$

$$y_s = (x_o + b_p/2)\sin\alpha_s - y_o \cos\alpha_s$$

with respect to the stator, where b_p is the distance between the two propeller planes. Since the pressure signal is determined by means of eq. 28, 29 and 30 in terms of $\sin\theta_1/r_1$ (i.e. in the transform ζ-plane), the transformation from the physical plane (x_r, y_r) or (x_s, y_s) is the next essential step. For a more systematic evaluation of the field point function $\sin\theta_1/r_1$ its contours for various values of (x_{rs}, y_{rs}) have been plotted in Fig. (3). This chart is derived from the Joukowski transformation

$$\zeta = z + \sqrt{z^2 - 1}$$

where $z = x + iy$, $\zeta = \xi + i\eta$, and x and y are expressed in terms of semi-chord at the effective radius. The following relations have been used in evaluating the contours of $\sin\theta_1/r_1$

$$x = \frac{\xi}{2}\left(1 + \frac{1}{\xi^2 + \eta^2}\right)$$

$$y = \frac{\eta}{2}\left(1 - \frac{1}{\xi^2+\eta^2}\right)$$

$$\eta = r_1 \sin\theta_1$$

$$\xi = r_1\cos\theta_1 - 1$$

The pressure signal due to interference effects between the two propellers can now be determined by means of eq. 28, 29 and 30 and by the contours of the field function $\sin\theta_1/r_1$.

Numerical calculations are made of the pressures along four longitudinal transverses at various axial distances for the propeller configuration 3-0-3 (no. 2714, see ref. 8) with the following pertinent characteristics

3-0-3 (No. 2714)
No. of blades, m = 3
Diameter, 2b = 0.68 ft.
Semi-chord, c , at 0.7b = 0.186 ft.
Distance between
propeller planes, b_p = 0.124 ft.
RPM = 900
Speed of advance = 8.16 ft/sec.

Results of these calculations are presented in Tables I and II. Table I gives the blade loading factor (ratio of unsteady dimensionless pressure to the field point function) for rotor and stator blades. Table II gives the field point function referred to rotor and stator blades for one position of the effective blade chord. From the products of stator or rotor blade-loading and field-point factors for a given x_o, y_o are obtained the steady and unsteady dimensionless pressure signals at that point, per blade of stator or rotor. Figure 4 shows the sum of the blade-frequency pressure signals due to rotor and stator blades plotted versus axial distance $x_o/D = x_o/2b$ for different tip clearances $r/b = y_o/b$. For the unsteady interference effects two circulation distributions are assumed, flat plate and elliptic. The results of Fig. 4 have been obtained for the blade chord center arbitrarily placed on the x_o-axis ($y_o = 0$).

If the pressure signal due to the interference effects is compared with the quasi-steady pressures computed by the method of Part I (see Table III) for the counterrotating system treated as though the two propellers operate as seperate units in three-dimensional flow, it is seen that up to a distance of 0.4 propeller radius, where the quasi-steady pressure (three-dimensional) attains its maximum, that pressure is at least 10 times the pressure signal due to the interference contribution. At larger distances, however, no conclusion can be drawn as to the relative magnitudes of the pressure signal contributed by the interference effect and of the quasi-steady signal because the rate of attenuation with axial distance of the two-dimensional pressure is considerably smaller than the rate of decay of the three-dimensional one. It can be stated, however, that in the actual three-dimensional case the interference effects will be smaller and will decay more rapidly.

To decide more conclusively about the relative importance of the interference effect a two-dimensional analogue of the uncoupled propeller configuration is considered. Expressions for the blade frequency pressure signal contributed by the forward and after string of blades operating independently have been developed by W. Jacobs by a procedure similar to that used in Reference 5 to determine the corresponding pressure due to the interference effects.

In Appendix D it is shown that the dimensionless pressure signals at a field point due to the motion of cascades of blades of the forward and after propeller operating independently are given as follows:

$$\frac{P^{(1)}}{T'} = -\frac{4\pi V_R}{m_B \Omega d}\,\frac{\sin\theta_1}{r_1}\,\mathrm{Re}\sum_m e^{i\alpha}\,e^{\pm im\nu t}\,[I_0(\lambda)+I_1(\lambda)]\left\{C(\mu)[J_0(\mu)-iJ_1(\mu)]+iJ_1(\mu)\right\} \tag{31}$$

ahd

$$\frac{P^{(2)}}{T'} = +\frac{4\pi V_R}{m_B \Omega d}\,\frac{\sin\theta_1}{r_1}\,\mathrm{Re}\sum_m e^{i\alpha}\,e^{\pm im\nu t}\,[I_0(\lambda)-I_1(\lambda)]\left\{C(\mu)[J_0(\mu)-iJ_1(\mu)]+iJ_1(\mu)\right\} \tag{32}$$

respectively,

where

m_B = number of blades

Ω = angular velocity = 2π (r.p.s.)

V_R = resultant velocity along the blade chord

$\lambda = \frac{2\pi mce^{i\alpha}}{d}$

$\mu = \frac{2\pi mce^{-i(\pi/2-\alpha)}}{d}$

and all geometric characteristics are measured at 0.7 propeller radius and are defined previously. Figure 5 graphically exhibits the comparison in a two-dimensional mathematical model of the total blade frequency pressure signal obtained from the motion of the two rows of blades operating separately with the pressure generated from the interference effects. It is seen from this figure that the propeller interference gives rise to a pressure signal at most 15% of the corresponding pressure obtained from the summation of the pressure fields of the two-rows of cascade blades operating as separate units (uncoupled). From the results it can be assumed, for practical purposes, that the additional pressure contributed by the mutual blade interference effects can be neglected.

The limited numerical results presented here indicate that:

1. the effect of the vortex wakes shed by the stator blades on the rotor (aft propeller) is comparable in magnitude to the effect induced by the stator (forward propeller) blades themselves,

2. the contribution of the rotor to the stator is small,

3. the interference part of the vibratory pressure signal is a small part of the total pressure signal in the near hydrodynamic field and can be neglected for the purpose of this analysis.

Part III

Calculation of the Pressure Field Near 3-0-3 Counterrotating Propellers

The vibratory pressure of various points in the neighborhood of a 3-0-3 counterrotating propeller is determined by utilizing the two expressions evolved in Part I for the pressure signal when the system of dual propellers is "in-phase" and "out-of-phase".

In figure (2a) the two 3-bladed propellers are shown to be located at $\pm x_o$ with respect to the origin of the coordinate system fixed on their common axis of rotation at the point midway between the propeller planes. In the computational work the two counterrotating components are No. 2714 propellers (Reference 8) whose pertinent characteristics have been given previously in Part II. The distance between them is taken as 0.364 of the propeller radius, i.e. $x_o = \pm 0.182$ in radii.

The locations at which the pressure signal is evaluated are given in the same figure. The pressure is computed along four longitudinal transverses having tip clearances $t/d = 0.1, 0.15, 0.20, 0.30$ and at 6 different stations along each layer, having axial distances: $x_o = 0$, 0.182, 0.382, 0.482, 0.582, and 0.782 of the propeller radius.

Expressions 11, 12, 14 and 15 which have been developed in Part I can be used in evaluating the harmonic coefficient of each individual propeller with special precaution being taken for the axial distance x. For the forward propeller the x is replaced by $x-x_o$ and for the after propeller by $x+x_o$, since the general expressions have been derived for the origin of the coordinate axes at a propeller center.

For several stations the coefficients of the first and second blade-frequencies were evaluated by the developed expressions and their values were found to be very close to those computed by numerical methods. However, as was mentioned before, the computational work was done in entirety on the ELECOM-100 computer, since the coding was available. The total pressure signal was determined by summing up the contributions

of three individual blades located at 120° intervals. Then the harmonic analysis was performed by the convenient numerical procedure described in Reference 4.

After the coefficients of the first and second harmonics are determined, the pressure signal in the field of the 3-0-3 counterrotating propeller is evaluated by using eq. (9) and (10), when blades are "in-phase" and "out-of-phase", respectively.

Results for the total amplitude of the first and second harmonics for the above two conditions have been plotted in Figures 6 and 7 versus tip clearances, at various axial distances.

Cross-plots of these results are shown in Figures 8, 9 and 10, where in addition the corresponding amplitudes of a single 3-bladed propeller producing equivalent thrust and having the same RPM have been plotted for comparison. The diameter of the conventional propeller has been determined by calculations made at theDavid Taylor Model Basin on the basis of the Troost optimum criteria, for SHP = 15,000 at 200 RPM. It is found on this basis that the diameter D_s of an equivalent single propeller is given in terms of the propeller diameter of the counterrotating system as

$$D_s = 1.25\, D_{CR}$$

Therefore the corresponding thrust loading coefficient T_s' of the single propeller will be given by

$$T_s' = \frac{T_s}{\frac{\pi}{4} D_s^2} = \frac{2T_{CR}}{\frac{\pi}{4} D_{CR}^2 (1.25)^2} = \frac{2}{(1.25)^2} T_{CR}' = 1.28\, T_{CR}'$$

The amplitudes of the pressure signal generated by the equivalent conventional propeller are evaluated at the same field points at which the pressure signals of the counterrotating system have been determined. The results of these calculations are presented in Tables III and IV as well as graphically in Figures 8, 9 and 10. This comparison indicates that for the first harmonic when the blades are in alignment the vibratory characteristics of the counterrotating configuration are undoubtedly

superior to the corresponding characteristics of the equivalent conventional single propeller in the immediate neighborhood of the propeller i.e. $x/b < 0.6$ and $t/d < 0.3$. Outside of that region, however, (see Fig. 8 and Table III) the equivalent single propeller is more advantageous since the counterrotating configuration in the "in-phase" condition acts as a single propeller with the same number of blades as one stage of the dual. In the out-of-phase situation, however, the counterrotating propeller system has always better vibratory characteristics than the equivalent single propeller as shown in Figures 9 and 10 and Tables III and IV. Since the in-phase situation is relatively infrequent, it can be generally stated that the counterrotating propeller configuration is superior to an equivalent conventional single propeller as far as the vibratory characteristics are concerned.

Of course, mechanical complications are involved in the counterrotating propeller configuration which are not overlooked in selecting the most advantageous configuration. It must also be pointed out, as was mentioned in the introduction, that other criteria, like the avoidance of cavitation, noise reduction, increase in efficiency, should be considered together with the vibratory characteristics in judging whether or not the advantages that are indicated for a counterrotating system counterbalance the disadvantages.

It is interesting to notice from the polar diagram (Figure 11) of the first blade harmonics of the pressure signal as a function of the observer's position relative to blade overlap, that the pressure at the lines of blade intersections (in-phase) has the frequency and the mode of a single propeller having the same number of blades as one stage of the dual, whereas in the direction midway between the intersection lines (out-of-phase) the pressure is that of a single propeller having the total number of blades of the set of two. In this figure the polar diagram of the pressure is made up of six loops since there are six overlaps of the counterrotating blades in one revolution. In the out-of-phase condition, there are six directions which coincide with the bisectors of the 60° intervals between overlaps.

CONCLUSIONS

This investigation indicates that the counterrotating propeller system has vibratory characteristics much superior to the equivalent single propeller having the same number of blades as one of its components, delivering the same thrust at the same RPM at optimum conditions. At a distance approximately 0.4 - 0.5 of the propeller diameter from the propeller plane the conventional propeller becomes better than the in-phase counterrotating system, but at instances when the blades are not in coincidence, a situation which occurs more often in a complete revolution, the superiority of the 3-0-3 system is evident at points farther away.

This study indicates also that the vibratory pressure signal of the counterrotating system can be obtained from the summation of the pressure fields of its two components, as though the two propellers operate as separate units, since their mutual interference effects calculated on the basis of 2-dimensional theory have been found to be a small part of the total pressure signal. In an actual three-dimensional situation, the contribution of the interference effect to the vibratory pressure signal will be smaller.

The study of the blade-blade interference effects in the two-dimensional analogue indicates that the effect on the aft propeller of the forward propeller with its shed vorticities is much more important than the effect of the aft propeller on the forward one, hence the latter effect can be omitted as negligible.

ACKNOWLEDGMENT

The authors wish to express their indebtedness to Miss Winnifred R. Jacobs for her assistance in performing some of the calculations and for her continuous interest and help in the preparation of this report.

REFERENCES

1. Breslin, J. P.: "The Pressure Field Near a Ship Propeller", Jour. of Ship Res., Vol. 1, No. 4, 1958.

2. Breslin, J.P. and Tsakonas, S.: "Marine Propeller Pressure Field Due to Loading and Thickness Effects", Trans. of SNAME, 1959, pp. 386- 422.

3. Breslin, J. P. and Tsakonas, S.: "The Blade Frequency Velocity Field Near an Operating Marine Propeller Due to Loading and Thickness Effects", Proc. of 6th Midwestern Conf. of Fluid Mechanics, Sept. 1959.

4. Breslin, J.P.: "The Unsteady Pressure Field Near a Ship Propeller and the Nature of Vibratory Forces Produced on an Adjacent Surface", ETT Report No. 609, June 1956.

5. Kemp, N. J. and Sears, W.R.: "Aerodynamic Interference Between Moving Blade Rows", Jour, of Aer. Sc., Vol. 20, No. 9, Sept. 1953.

6. Kussner, H. G. and Schwarz, L.: "The Oscillating Wing with Aerodynamic Balanced Elevator", NACA RM 991 (1941).

7. Fung, Y.C.: "An Introduction to the Theory of Aeroelasticity", Published by John Wiley.

8. Tachmindji, A.J. and Dickerson, M.C.: "The Measurement of the Oscillating Pressures in the Vicinity of Propellers", DTMB Rep. 1130, Apr. 1957.

9. Tsakonas, S., Breslin, J.P. and Chen, C.Y.; "The Sound Pressure Field Generated by a Marine Propeller Operating in a Wake", D.L. Report 832, February 1961.

10. Tsakonas, S.: "Analytical Expressions for Thrust Deduction and Wake Fraction for Potential Flows", Jour. Ship Res., Vol. 2, No. 1, June 1958.

TABLE I

$\frac{P_r}{T'} / \left(\frac{\sin\theta_1}{r_1}\right)_r$ per blade of rotor for $J = 0.8$

Blade Harmonics	With Flat Plate Distribution of Circulation	With Elliptic Distribution of Circulation
	1) Effect of steady circulation of stator	
1	-.057 + i.005	-.049 + i.138
2	i.006	.002 + i.019
3	i.001	.001 + i.006
	2) Effect of Wake Vorticities Shed by Stator	
1	+.010 + i.027	.022 + i.010
2	-.004 - i.037	-.022 - i.002

$\frac{P_s}{T'} / \left(\frac{\sin\theta_1}{r_1}\right)_s$ per blade of stator for $J = 0.8$

	1) Effect of Steady circulation of rotor	
1	-.001 - i.026	-.021 - i.001
2	-.001 - i.008	-.002
3	-.001 - i.003	---

TABLE II

Field point function $(\frac{\sin\theta_1}{r_1})$ referred to rotor and stator blades

(center of blade chord on x_o-axis)

y_o/R ($\equiv r/R$)	x_o/R	$(\frac{\sin\theta_1}{r_1})_r$	$(\frac{\sin\theta_1}{r_1})_s$
1.2	0	.030	.200
	.182	.050	.167
	.382	.073	.120
	.488	.077	.083
	.582	.081	.050
	.782	.093	-.005
	1.6	.093	-.080
	2.0	.088	-.080
	3.0	.083	-.070
	4.0	.060	-.055
	6.0	.042	-.039
	8.0	.033	-.030
1.4	0	.023	.150
	.182	.038	.133
	.382	.055	.100
	.488	.062	.073
	.582	.067	.050
	.782	.080	.013
	1.6	.090	-.060
1.6	0	.019	.130
	.182	.033	.111
	.382	.044	.080
	.488	.050	.067
	.582	.055	.050
	.782	.067	.020
	1.6	.087	-.040

TABLE III

First Blade Harmonics of Pressure Signal P/T'_{CR} due to

1) 3-0-3 counterrotating propellers of radius b

2) 3-bladed single propeller of radius 1.25b (equivalent thrust)

Field point position		3-0-3 in-phase	3-0-3 out-of-phase	Single
x_o/b	r/b	P/T'_{CR}*	P/T'_{CR}*	P/T'_{CR}*
0	1.2	.083	.135	.070
	1.3	.060	.072	.071
	1.4	.044	.041	.051
	1.6	.026	.015	.029
.182	1.2	.097	.063	.47
	1.3	.068	.041	.23
	1.4	.048	.026	.094
	1.6	.027	.012	.035
.382	1.2	.12	.041	.16
	1.3	.078	.019	.12
	1.4	.054	.010	.087
	1.6	.028	.006	.041
.488	1.2	.10	.044	.11
	1.3	.071	.024	.092
	1.4	.050	.013	.071
	1.6	.027	.005	.036
.582	1.2	.082	.039	.086
	1.3	.061	.024	.072
	1.4	.045	.015	.055
	1.6	.026	.006	.032
.782	1.2	.047	.024	.041
	1.3	.039	.017	.035
	1.4	.031	.012	.030
	1.6	.020	.006	.020

*Subscript CR refers to counterrotating propellers

TABLE IV

Second Blade Harmonics of Pressure Signal P/T'_{CR} due to

1) 3-0-3 counterrotating propeller of radius b

2) 3-bladed single propeller of radius 1.25b (equivalent thrust)

Field point position		3-0-3 (in-phase or out-of-phase)	Single
x_o/b	r/b	P/T'_{CR*}	P/T'_{CR*}
0	1.2	.032	.027
	1.3	.019	.043
	1.4	.011	.028
	1.6	.004	.011
.182	1.2	.035	.23
	1.3	.020	.12
	1.4	.011	.056
	1.6	.005	.013
.382	1.2	.041	.054
	1.3	.021	.045
	1.4	.012	.032
	1.6	.004	.012
.488	1.2	.028	.035
	1.3	.017	.029
	1.4	.010	.021
	1.6	.004	.009
.582	1.2	.018	.021
	1.3	.012	.017
	1.4	.008	.012
	1.6	.003	.006
.782	1.2	.007	.007
	1.3	.005	.005
	1.4	.004	.004
	1.6	.002	.003

*Subscript CR refers to counterrotating propellers

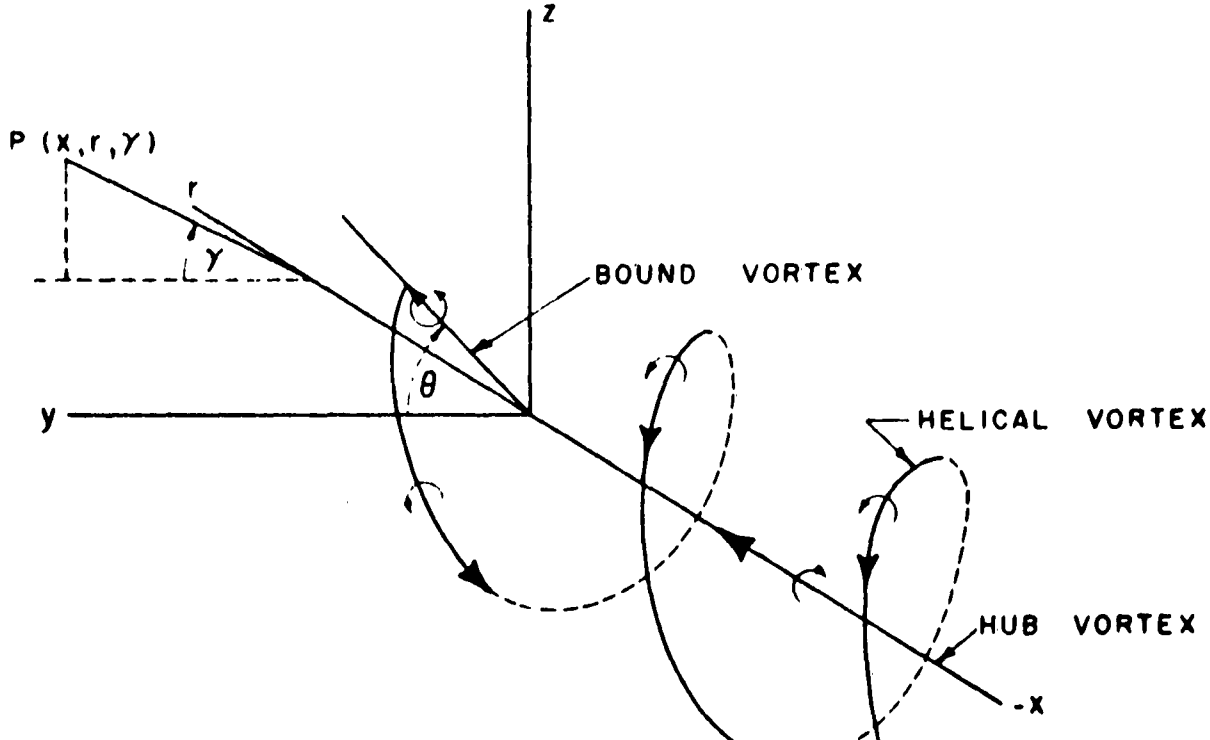

FIGURE I. ARRANGEMENT OF AXES AND VORTEX REPRESENTATION OF PROPELLER

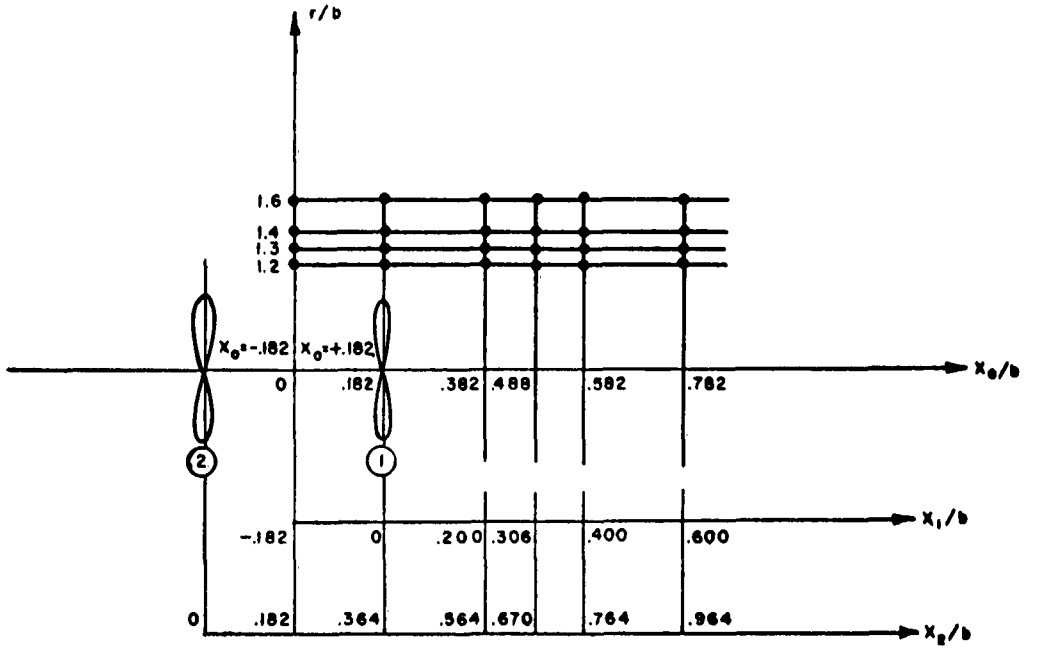

FIGURE 2a. COORDINATE SYSTEM WITH FIELD POINTS FOR WHICH CALCULATIONS ARE PRESENTED

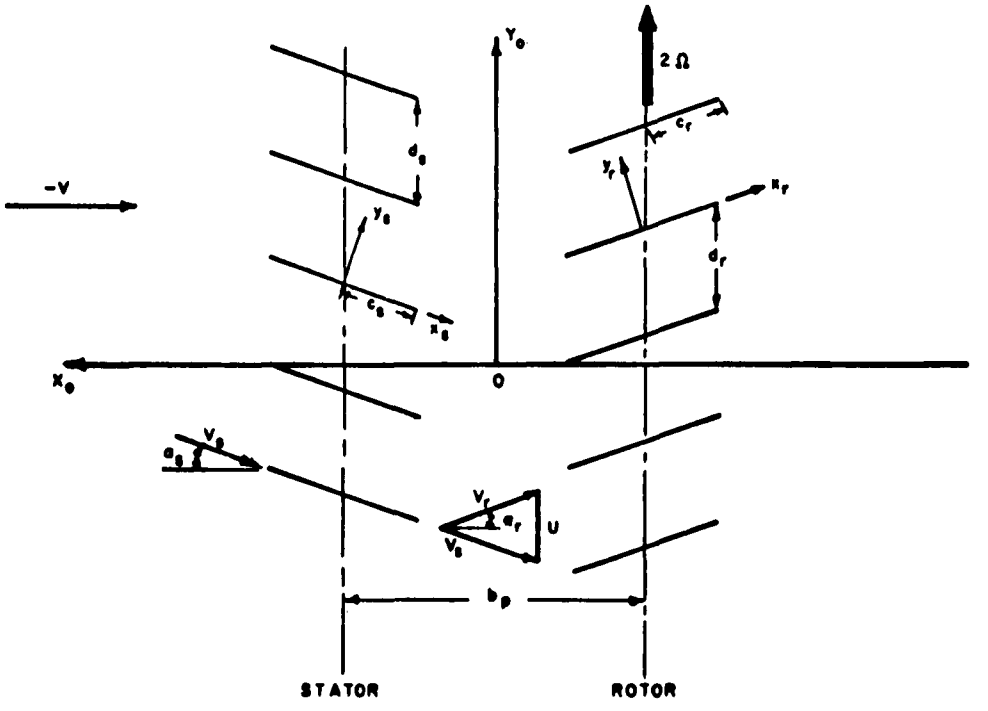

FIGURE 2b. BLADE ARRANGEMENT OF TWO-DIMENSIONAL ANALOGUE FOR COUNTERROTATING PROPELLER CONFIGURATION

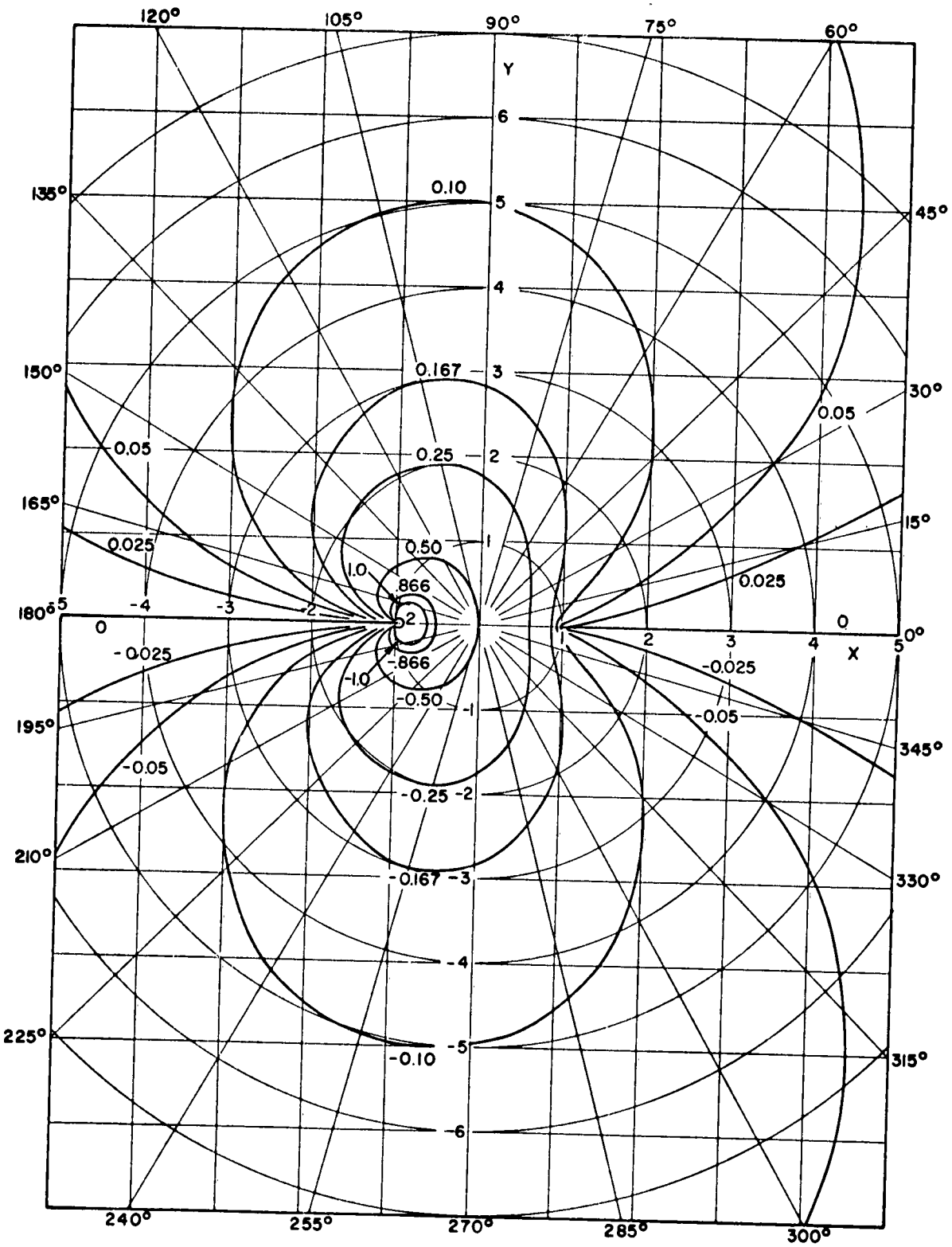

FIGURE 3. CONTOURS OF $\frac{\text{SIN } \theta_1}{r_1}$, FOR VARYING X, Y, $r = \sqrt{X^2 + Y^2}$ AND θ = ARC TAN Y/X

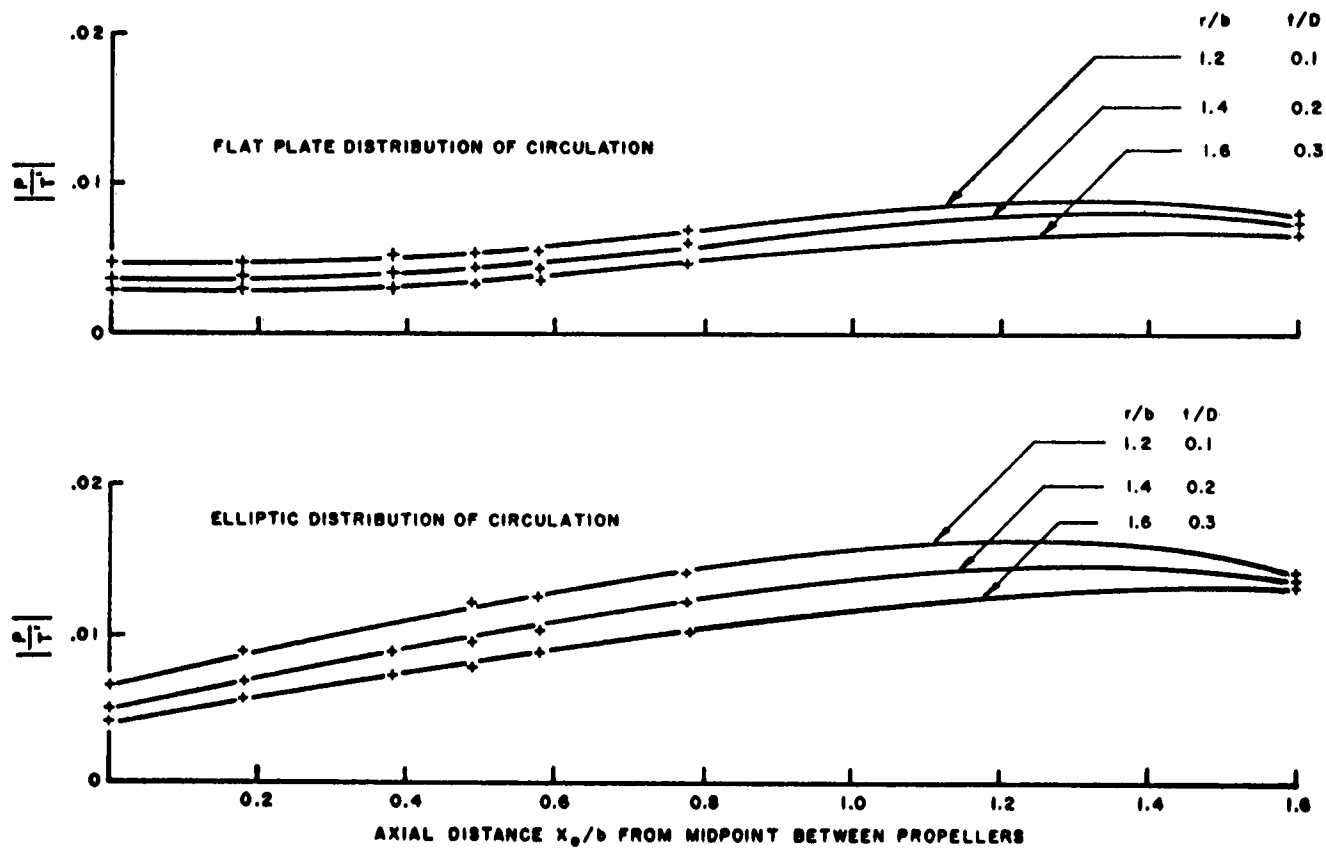

FIGURE 4. AMPLITUDE OF THE 1st BLADE HARMONIC OF THE UNSTEADY DIMENSIONLESS PRESSURE SIGNAL P/T' PER BLADE DUE TO INTERFERENCE EFFECTS, FOR A TWO-DIMENSIONAL MATHEMATICAL MODEL REPRESENTING THE COUNTERROTATING SYSTEM. (J= 0.8, CENTER OF BLADE CHORD ON X_0 - AXIS)

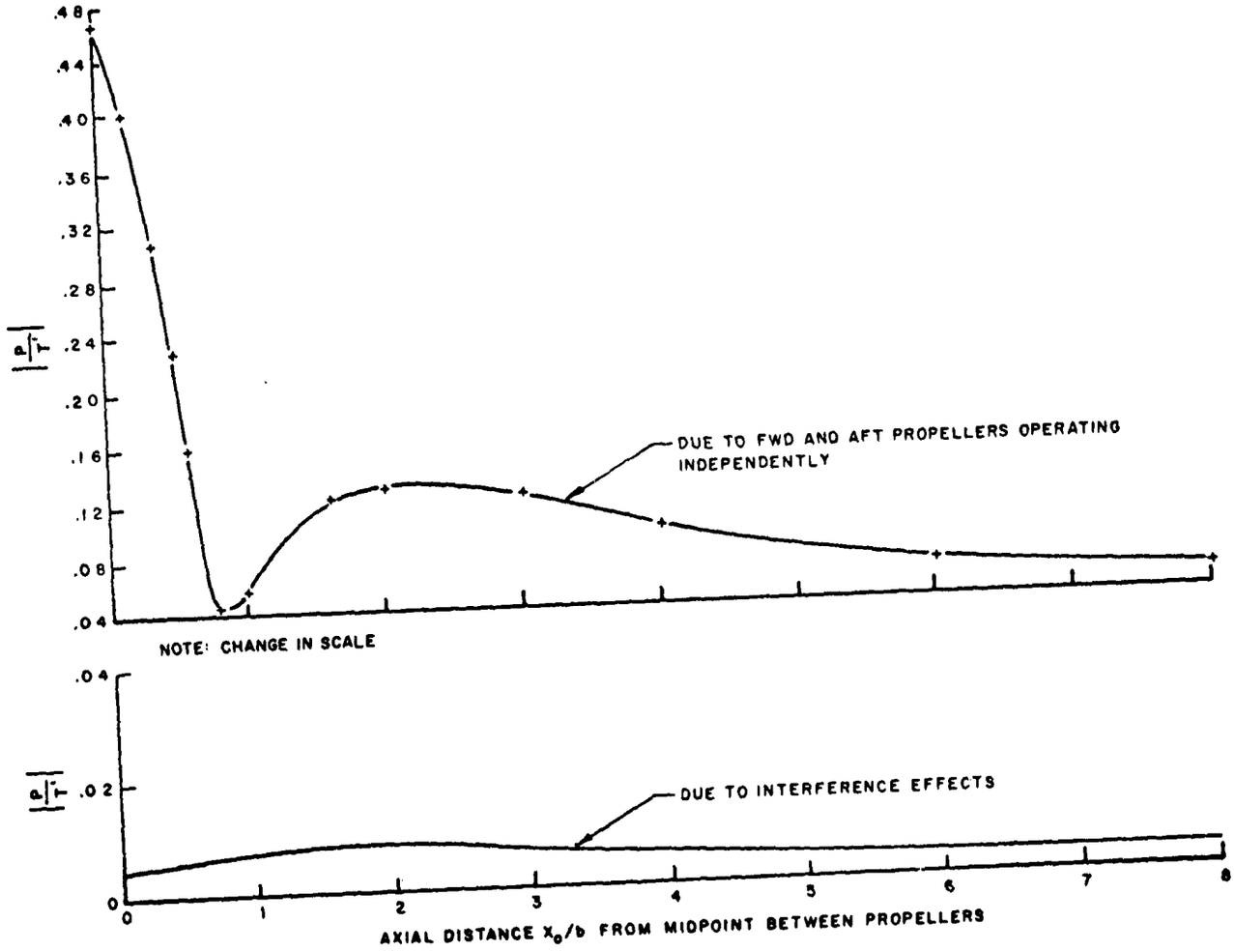

FIGURE 5. AMPLITUDES OF THE 1st BLADE HARMONIC OF THE UNSTEADY DIMENSIONLESS PRESSURE SIGNALS PER BLADE DUE TO THE COUNTERROTATING SYSTEM REPRESENTED BY A TWO-DIMENSIONAL MATHEMATICAL MODEL WITH FLAT-PLATE CIRCULATION DISTRIBUTION. ($J = 0.8$, $r/b = 1.2$, $1/D = 0.1$)

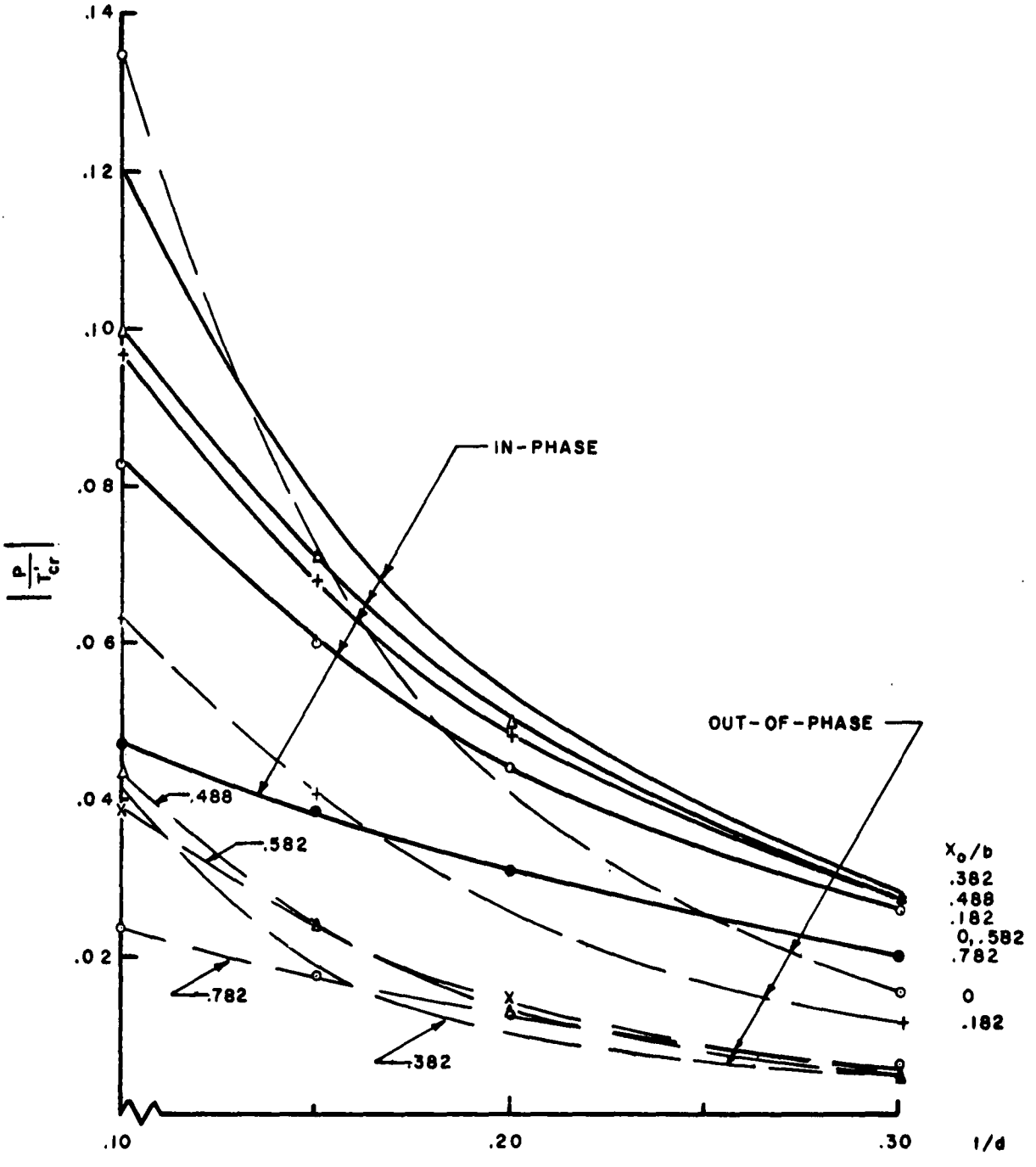

FIGURE 6. AMPLITUDES OF THE 1st BLADE HARMONIC OF THE DIMENSIONLESS PRESSURE |P/T'| DUE TO THE UNCOUPLED COUNTERROTATING SYSTEM FOR THE IN AND OUT-OF-PHASE CONDITIONS

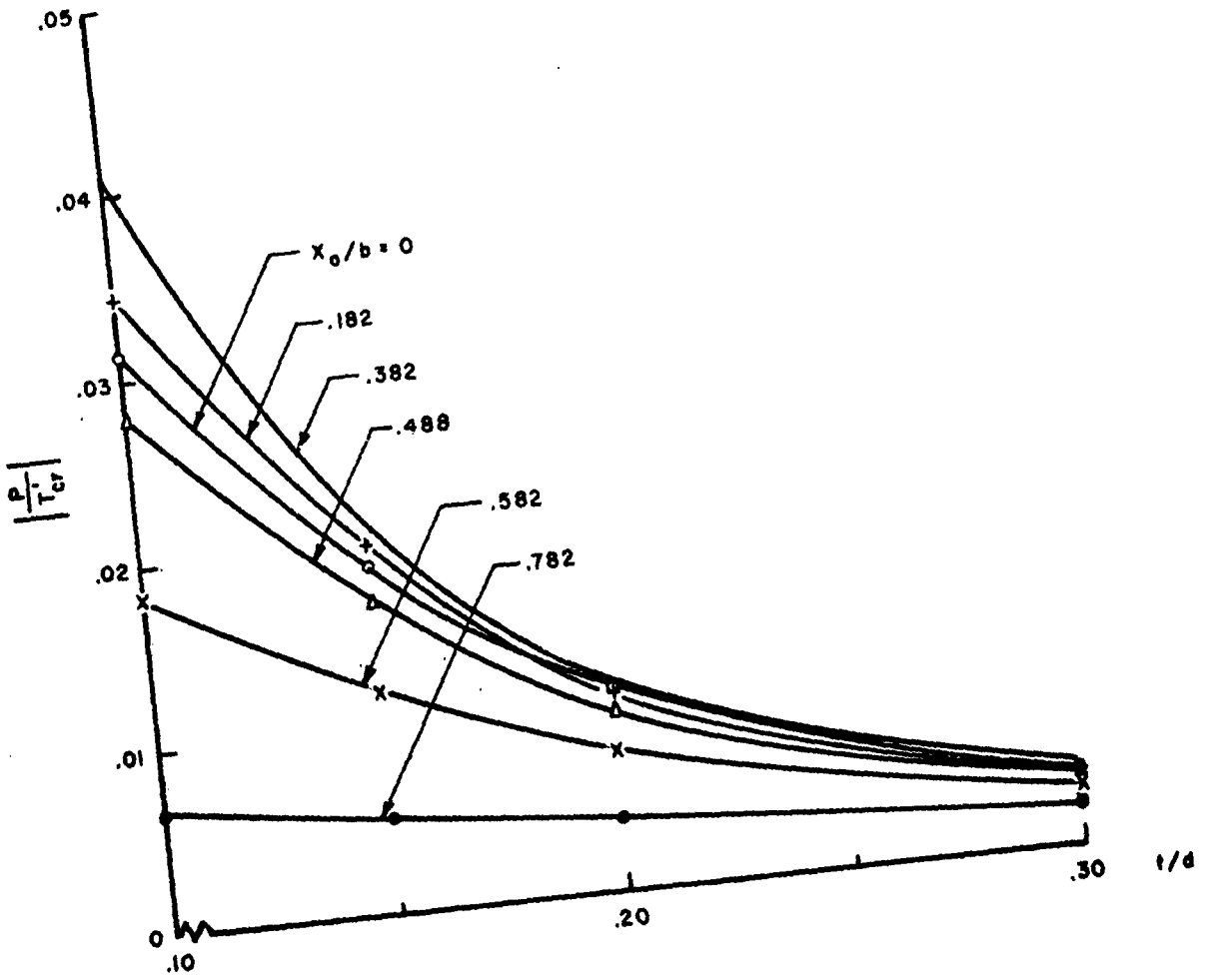

FIGURE 7. AMPLITUDES OF THE 2nd BLADE HARMONIC OF THE DIMENSIONLESS PRESSURE |P/T'| DUE TO THE UNCOUPLED COUNTERROTATING SYSTEM, IN AND OUT-OF-PHASE

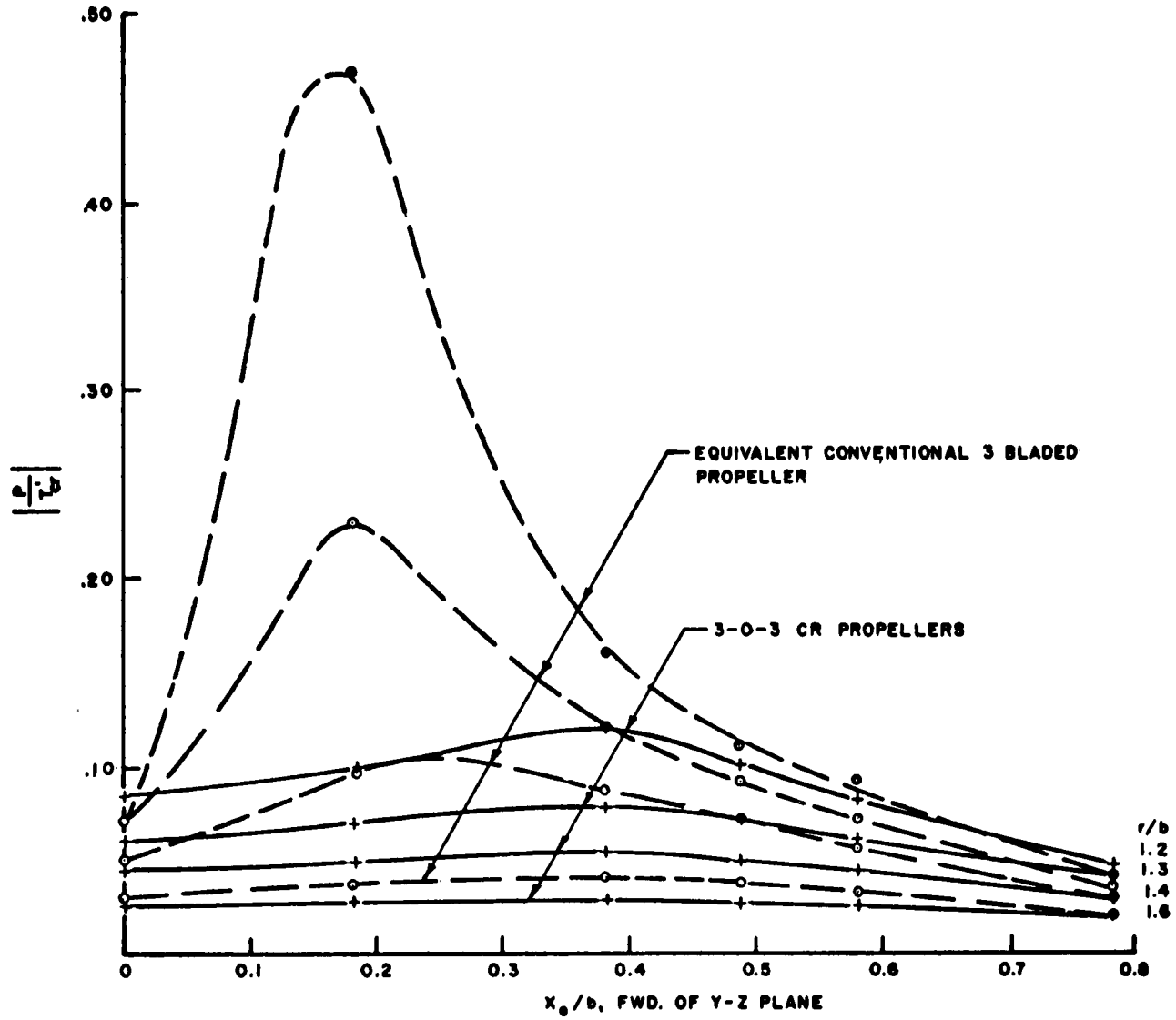

FIGURE 8. COMPARISON OF AMPLITUDES OF THE 1st BLADE HARMONIC OF THE DIMENSIONLESS PRESSURE DUE TO THE COUNTERROTATING SYSTEM IN THE IN-PHASE CONDITION WITH THOSE DUE TO THE EQUIVALENT CONVENTIONAL PROPELLER

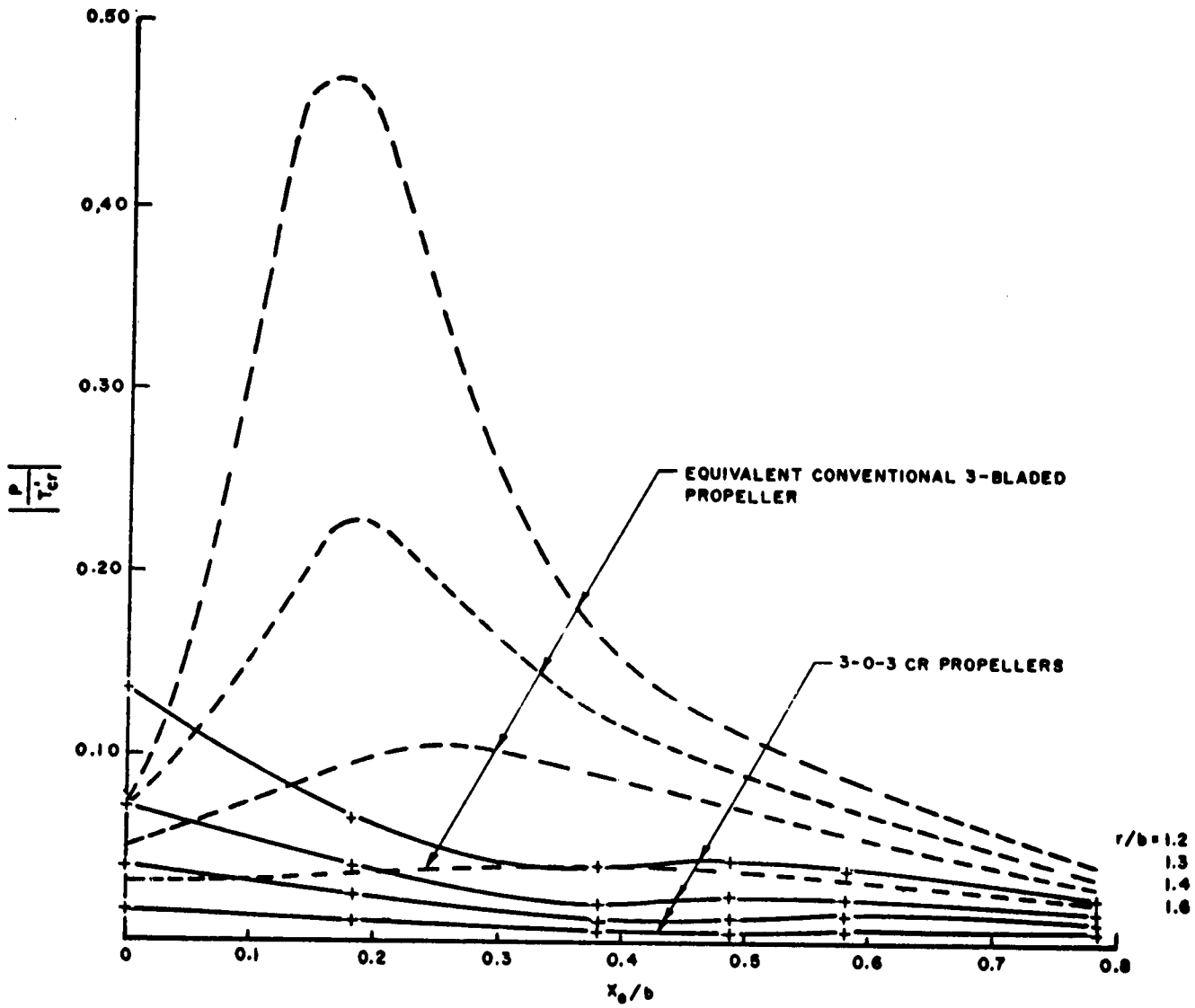

FIGURE 9. COMPARISON OF AMPLITUDES OF THE 1st BLADE HARMONIC OF THE DIMENSIONLESS PRESSURE DUE TO THE COUNTERROTATING SYSTEM IN THE OUT-OF-PHASE CONDITION WITH THOSE DUE TO THE EQUIVALENT CONVENTIONAL PROPELLER

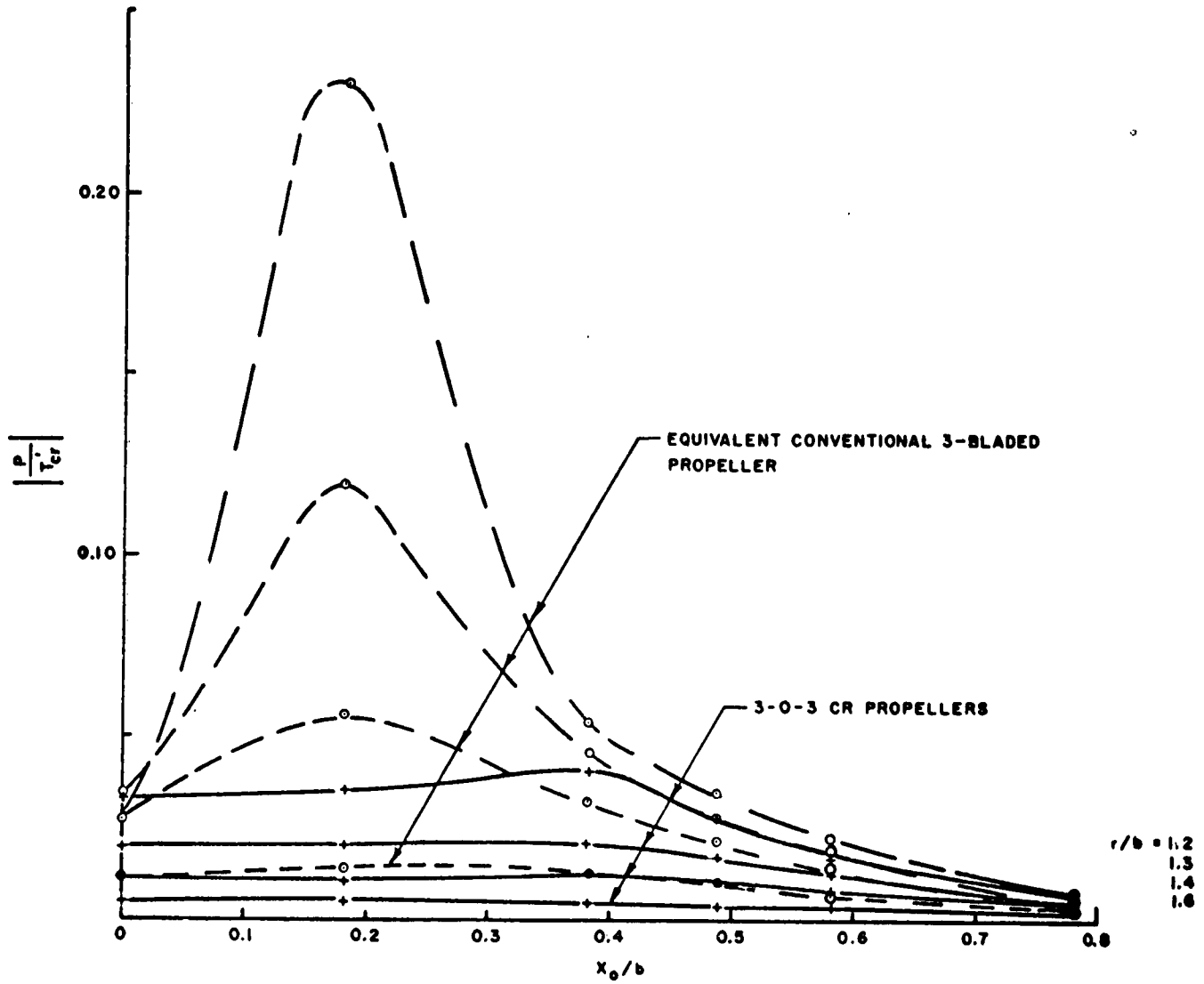

FIGURE 10. COMPARISON OF AMPLITUDES OF THE 2nd BLADE HARMONIC OF THE DIMENSIONLESS PRESSURE DUE TO THE COUNTERROTATING SYSTEM, IN AND OUT-OF-PHASE, WITH THOSE DUE TO THE EQUIVALENT CONVENTIONAL PROPELLER

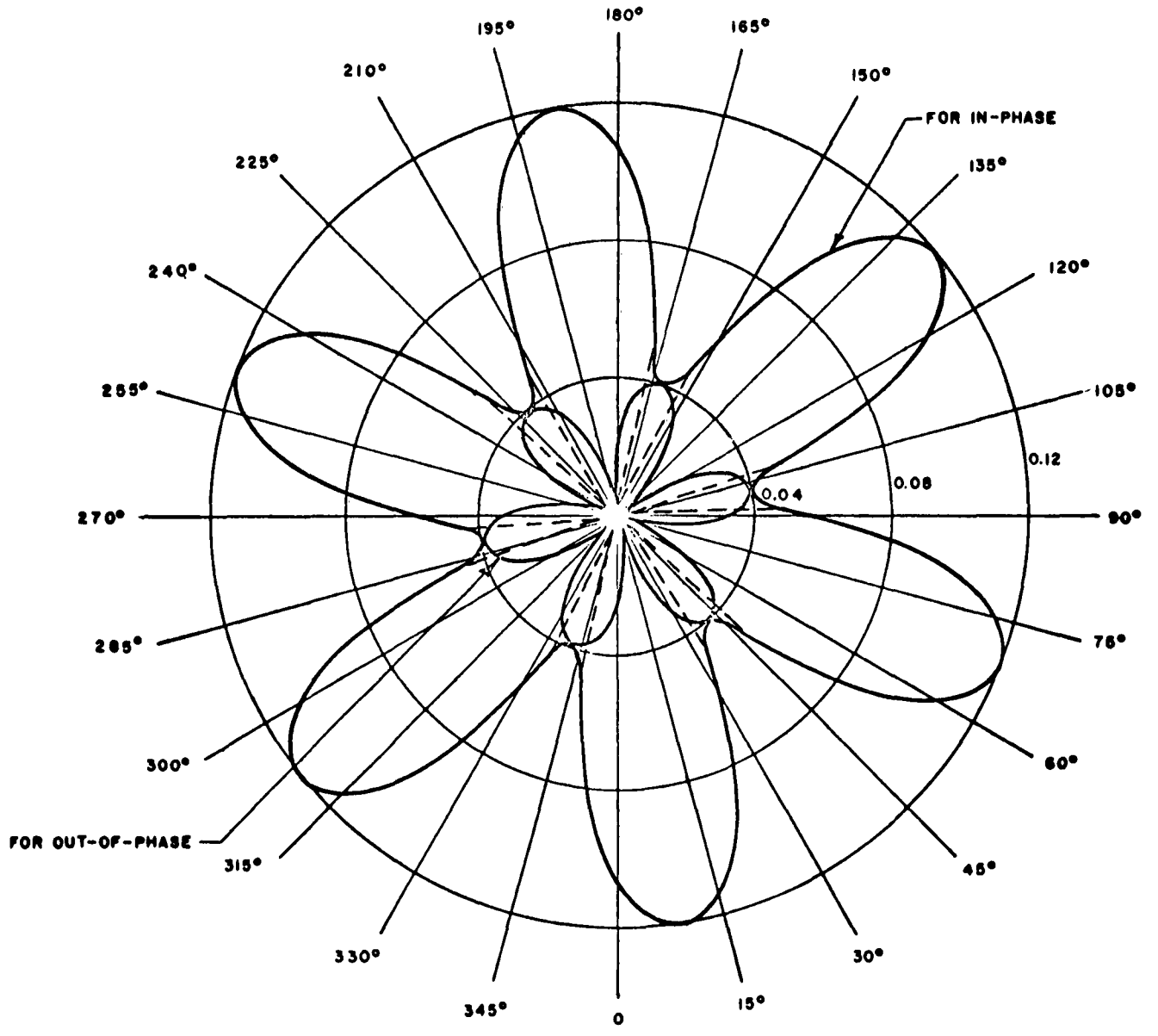

FIGURE 11. POLAR DIAGRAM OF THE 1st BLADE HARMONIC OF THE DIMENSIONLESS PRESSURE DUE TO THE COUNTERROTATING SYSTEM, IN THE IN AND OUT-OF-PHASE CONDITIONS, AT $\bar{r}/b = 1.2$, $X_0/b = 0.382$

APPENDIX A

It is known that the sum of a finite geometric series,

$$1+z+z^2+\ldots.z^n = \frac{1-z^{n+1}}{1-z}$$

If $z = e^{i\theta}$, it can be shown that

$$\cos\theta+\cos 2\theta+\ldots \cos n\theta = -\frac{1}{2} + \frac{\sin[(n+1/2)\theta)]}{2\sin\theta/2}$$

$$\sin\theta+\sin 2\theta+\ldots \sin n\theta = \frac{1}{2}\cot\theta/2 - \frac{\cos[(n+1/2)\theta]}{2\sin\theta/2}$$

These identities are used to prove that the vibratory pressure is made up of all the harmonics whose order is an integer multiple of the number of blades.

The cosine part of the pressure distribution is given by

$$\frac{mP}{T'} = \sum_{k=0}^{\infty} A_k \cos k\alpha + \sum_{n=1}^{m-1}\sum_{k=0}^{\infty} A_k \cos k\left(\alpha + \frac{2\pi}{m}n\right)$$

where the first term is due to the first blade and the second is due to the remaining (m-1) blades.

It can be shown that

$$\sum_{n=1}^{m-1} \cos k\left(\alpha + \frac{2\pi}{m}n\right) = \begin{cases} (-1)\cos k\alpha & \text{when } k \neq \text{integer multiple of } m \\ (m-1)\cos k\alpha & \text{when } k = \text{integer multiple of } m \end{cases}$$

Proof:

$$\sum_{n=1}^{m-1} \cos k\left(\alpha + \frac{2\pi}{m} n\right) = \sum_{n=1}^{m-1} \left[\cos k\alpha \cos k\frac{2\pi}{m} n - \sin k\alpha \sin k\frac{2\pi}{m} n\right]$$

$$= \cos k\alpha \left\{\cos \frac{k2\pi}{m} + \cos 2\frac{k2\pi}{m} + \cdots + \cos(m-1)\frac{k2\pi}{m}\right\}$$

$$- \sin k\alpha \left\{\sin \frac{k2\pi}{m} + \sin 2\frac{k2\pi}{m} + \cdots + \sin (m-1)\frac{k2\pi}{m}\right\}$$

$$= \cos k\alpha \left\{-\frac{1}{2} + \frac{\sin\left[m-1+\frac{1}{2}\right)\frac{k2\pi}{m}\right]}{2\sin\frac{k\pi}{m}}\right\}$$

$$- \sin k\alpha \left\{\frac{1}{2}\cot\frac{k\pi}{m} - \frac{\cos\left[(m-1+\frac{1}{2})\frac{k2\pi}{m}\right.}{2\sin\frac{k\pi}{m}}\right\}$$

$$= \cos k\alpha \left\{-\frac{1}{2} + \frac{\sin 2\pi k \cos\frac{k\pi}{m} - \cos 2\pi k \sin\frac{\pi k}{m}}{2\sin\frac{k\pi}{m}}\right\}$$

$$- \sin k\alpha \left\{\frac{1}{2}\cot\frac{k\pi}{m} - \frac{\cos 2\pi k \cos\frac{\pi k}{m} + \sin 2\pi k \sin\frac{\pi k}{m}}{2\sin\frac{k\pi}{m}}\right\}$$

$$= \cos k\alpha \left\{-\frac{1}{2} + \frac{-\sin\frac{\pi k}{m}}{2\sin\frac{\pi k}{m}}\right\} - \sin k\alpha \left\{\frac{1}{2}\cot\frac{k\pi}{m} - \frac{\cos\frac{\pi k}{m}}{2\sin\frac{k\pi}{m}}\right\}$$

$= \cos k\alpha\,(-1) - \sin k\alpha\,(0) = -\cos k\alpha$ provided that $k \neq$ integer multiple of m.

Then $\frac{mP}{T'} = \sum_{k=0}^{\infty} [A_k \cos k\alpha - A_k \cos k\alpha] = 0$ (no pressure signal) if k ≠ integer multiple of m .

If k = integer multiple of m

$$\sum_{n=1}^{m-1} \cos k\left(\alpha + \frac{2\pi}{m} n\right) = \sum_{n=1}^{m-1} [\cos k\alpha \cos 2\pi n - \sin k\alpha \sin 2\pi n]$$

$$= \sum_{n=1}^{m-1} \cos k\alpha \cos 2\pi n = (m-1) \cos k\alpha$$

Then

$$\frac{mP}{T'} = \sum_{k=0}^{\infty} [A_k \cos k\alpha + A_k (m-1) \cos k\alpha] = \sum_{k=1}^{\infty} A_k m \cos k\alpha$$

or

$$\frac{\text{Total pressure}}{T'} = \sum_{k=1}^{\infty} A_{km} \cos km\alpha$$

The sine part of the pressure distribution is

$$\frac{mP}{T'} = \sum_{k=0}^{\infty} B_k \sin k\alpha + \sum_{n=1}^{m-1} \sum_{k=0}^{\infty} B_k \sin k\left(\alpha + \frac{2\pi n}{m}\right)$$

$$\sum_{n=1}^{m-1} \sin k\left(\alpha + \frac{2\pi n}{m}\right) = \sum_{n=1}^{m-1} \left[\cos k\alpha \sin k \frac{2\pi}{m} n + \sin k\alpha \cos k \frac{2\pi n}{m}\right]$$

$$= \cos k\alpha \left[\frac{1}{2} \cot \frac{k\pi}{m} - \frac{\cos (m-1/2) \frac{k2\pi}{m}}{2 \sin \frac{k\pi}{m}}\right]$$

$$+ \sin k\alpha \left[-\frac{1}{2} + \frac{\sin(m-1/2)\frac{k2\pi}{m}}{2 \sin \frac{k\pi}{m}} \right]$$

$= -\sin k\alpha$ for $k \neq$ integer multiple of m and $P = 0$.

If k = integer multiple of m, it can be shown that

$$\sum_{n=1}^{m-1} \sin k\left(\alpha + \frac{2\pi n}{m}\right) = (m-1) \sin k\alpha$$

Then $$\frac{mP}{T'} = m \sum_{k=0}^{\infty} B_k \sin k\alpha$$

$$\frac{P}{T'} = \sum_{k=1}^{\infty} B_{km} \sin km\alpha$$

APPENDIX B

Expressions for the pressure signal due to a system of counterrotating propellers will be developed at the instances when the blades are in coincidence, "in phase", and in the "out-of-phase" position. For the "in-phase" condition $t = \frac{\pi}{m\omega}$, whereas the out-of-phase situation occurs when $t = \frac{\pi}{2m\omega}$.

The pressure signal, restricted to the first and second blade harmonics, is

$$\frac{P}{T'} = A_m^{(1)} \cos m\alpha_1 + A_{2m}^{(1)} \cos 2m\alpha_1 + B_m^{(1)} \sin m\alpha_1 + B_{2m}^{(1)} \sin 2m\alpha_1$$

$$A_m^{(2)} \cos m\alpha_2 + A_{2m}^{(2)} \cos 2m\alpha + B_m^{(2)} \sin m\alpha_2 + B_{2m}^{(2)} \sin 2m\alpha_2$$

When $t = \frac{\pi}{m\omega}$

$$A_m^{(2)} \cos m\alpha_2 = A_m^{(2)} \cos m(\alpha_1 - 2\omega t) =$$

$$= A_m^{(2)} \cos m\alpha_1$$

$$A_{2m}^{(2)} \cos 2m\alpha_2 = A_{2m}^{(2)} \cos 2m(\alpha_1 - 2\omega t) =$$

$$= A_{2m}^{(2)} \cos 2m\alpha_1$$

$$B_m^{(2)} \sin m\alpha_2 = B_m^{(2)} \sin m(\alpha_1 - 2\omega t) =$$

$$= B_m^{(2)} \sin m\alpha_1$$

$$B_{2m}^{(2)} \sin 2m\,\alpha_2 = B_{2m}^{(2)} \sin 2m(\alpha_1 - 2\omega t)$$

$$= B_{2m}^{(2)} \sin 2m\alpha_1$$

Therefore

$$\frac{P^{(1)}+P^{(2)}}{T'} = \left\{(A_m^{(1)} + A_m^{(2)}) \cos m\alpha_1 + (A_{2m}^{(1)} + A_{2m}^{(2)} \cos 2m\,\alpha_1 + (B_m^{(1)} + B_m^{(2)}) \sin m\alpha_1 + (B_{2m}^{(1)} + B_{2m}^{(2)}) \sin 2m\,\alpha_1\right\}$$

or

$$\frac{P^{(1)}+P^{(2)}}{T'} = \sqrt{(A_m^{(1)} + A_m^{(2)})^2 + (B_m^{(1)} + B_m^{(2)})^2} \cos(m\alpha_1 - \varepsilon_1) + \sqrt{(A_{2m}^{(1)} + A_{2m}^{(2)})^2 + (B_{2m}^{(1)} + B_{2m}^{(2)})^2} \cos(2m\alpha_1 - \varepsilon_2)$$

where $\varepsilon_1 = \tan^{-1} \frac{B_m^{(1)} + B_m^{(2)}}{A_m^{(1)} + A_m^{(2)}}$ and $\varepsilon_2 = \tan^{-1} \frac{B_{2m}^{(1)} + B_{2m}^{(2)}}{A_{2m}^{(1)} + A_{2m}^{(2)}}$

The out-of-phase condition occurs at

$$t = \frac{\pi}{2\pi\omega}$$

hence

$$A_m^{(2)} \cos m\alpha_2 = A_m^{(2)} \cos m(\alpha_1 - 2\omega t)$$

$$= -A_m^{(2)} \cos m\alpha_1$$

$$A_{2m}^{(2)} \cos 2m\,\alpha_2 = A_{2m}^{(2)} \cos 2m(\alpha_1 - 2\omega t) =$$

$$= A_{2m}^{(2)} \cos 2m\,\alpha_1$$

$$B_m^{(2)} \sin m\,\alpha_2 = B_m^{(2)} \sin m(\alpha_1 - 2\omega t)$$

$$= - B_m^{(2)} \sin m \alpha_1$$

$$B_{2m}^{(2)} \sin 2m \alpha_2 = B_{2m}^{(2)} \sin 2m (\alpha_1 - 2\omega t)$$

$$= B_{2m}^{(2)} \sin 2m \alpha_1$$

Therefore

$$\frac{P^{(1)} + P^{(2)}}{T'} = (A_m^{(1)} - A_m^{(2)}) \cos m \alpha_1 + (A_{2m}^{(1)} + A_{2m}^{(2)}) \cos 2m \alpha_1$$

$$+ (B_m^{(1)} - B_m^{(2)}) \sin m \alpha_1 + (B_{2m}^{(1)} + B_{2m}^{(2)}) \sin 2m\alpha$$

or

$$\frac{P^{(1)} + P^{(2)}}{T'} = \sqrt{(A_m^{(1)} - A_m^{(2)})^2 + (B_m^{(1)} - B_m^{(2)})^2} \cos (m\alpha_1 - \varepsilon_3)$$

$$+ \sqrt{(A_{2m}^{(1)} + A_{2m}^{(2)})^2 + (B_{2m}^{(1)} + B_{2m}^{(2)})^2} \cos (2m\alpha_1 - \varepsilon_4)$$

where $\varepsilon_3 = \tan^{-1} \dfrac{B_m^{(1)} - B_m^{(2)}}{A_m^{(1)} - A_m^{(2)}}$

$$\varepsilon_4 = \tan^{-1} \frac{B_{2m}^{(1)} + B_{2m}^{(2)}}{A_{2m}^{(1)} + A_{2m}^{(2)}} = \varepsilon_2$$

APPENDIX C

The derivation of the Fourier coefficients of the second blade frequency of the pressure signal near a three-bladed propeller given by eq. (14) and (15) will be shown in very general steps and the most representative type of integration will be carried out.

After the designated integration with respect to s the instantaneous pressure signal given by eqs. (1) and (2) becomes

$$\frac{P}{T'} = C_2[I_1 - I_2 - I_3 + I_4] + C_1[I_5 - I_6 + I_7] \qquad \text{(C-1)}$$

where $C_2 = 1/2$ $\quad C_1 = J/2\pi$

$$I_1 = \frac{x}{e^{1/2}} \qquad I_2 = \frac{x(x^2+r^2)^{1/2}}{a} \qquad I_3 = \frac{xr\cos\alpha}{a\, e^{1/2}} \qquad I_4 = \frac{xr^2\cos^2\alpha}{a\, e^{1/2}}$$

$$I_5 = \frac{r^2\sin\alpha\cos\alpha}{a\, e^{1/2}} \qquad I_6 = \frac{r\sin\alpha}{a\, e^{1/2}} \qquad I_7 = \frac{r^2\sin\alpha\cos\alpha}{(x^2+r^2)^{1/2} a}$$

$$e = 1 + x^2 + r^2 - 2r\cos\alpha \quad \text{and} \quad a = x^2 + r^2\sin^2\alpha$$

To evaluate the second harmonic of expression (C-1) it is necessary to find the sine and cosine Fourier coefficients. The cosine coefficients are:

$$a_1 = \frac{1}{\pi}\int_{-\pi}^{\pi} \frac{x\cos 6\alpha\, d\alpha}{e^{1/2}}$$

$$a_2 = \frac{1}{\pi}\int_{-\pi}^{\pi} \frac{x(x^2+r^2)^{1/2}\cos 6\alpha\, d\alpha}{a}$$

$$a_3 = \frac{1}{\pi}\int_{-\pi}^{\pi} \frac{xr\cos\alpha\cos 6\alpha\, d\alpha}{a\, e^{1/2}}$$

$$a_4 = \frac{1}{\pi}\int_{-\pi}^{\pi} \frac{xr^2\cos^2\alpha\,\cos 6\alpha\, d\alpha}{a\,e^{1/2}}$$

$a_5 = a_6 = a_7 = 0$ since the integrands are odd functions with respect to angle α.

The corresponding sine coefficients are:

$B_1 = B_2 = B_3 = B_4 = 0$, since they are odd functions with respect to α.

$$B_5 = \frac{1}{\pi}\int_{-\pi}^{\pi} \frac{r^2\sin\alpha\cos\alpha\sin 6\alpha\, d\alpha}{a\,e^{1/2}}$$

$$B_6 = \frac{1}{\pi}\int_{-\pi}^{\pi} \frac{r\,\sin\alpha\sin 6\alpha\, d\alpha}{a\,e^{1/2}}$$

$$B_7 = \frac{1}{\pi}\int_{-\pi}^{\pi} \frac{r^2\sin\alpha\cos\alpha\sin 6\alpha\, d\alpha}{(x^2+r^2)^{1/2}\,a}$$

$a_1, a_2 \ldots\ldots a_7$ and $B_1, B_2 \ldots\ldots B_7$ are the cosine and sine coefficients of the components $(I_1, I_2 \ldots\ldots I_7)$ of eq. (C-1)
On expanding $\cos 6\alpha$ and $\sin 6\alpha$ in terms of $\cos\alpha$ and $\sin\alpha$ the following representative types of integral will occur:

$$C_m = \int_{-\pi}^{\pi} \frac{\cos^m\alpha\, d\alpha}{(1+x^2+r^2-2r\cos\alpha)^{1/2}}$$

where m (integer) = 0 6

$$D_m = \int_{-\pi}^{\pi} \frac{\cos^m \alpha \, d\alpha}{x^2 + r^2 \sin^2 \alpha} \qquad m \text{ (integer)} = 0,\ 2,\ 4,\ 6,\ 8$$

$$E_m = \int_{-\pi}^{\pi} \frac{\cos^m \alpha \, d\alpha}{(x^2 + r^2 \sin^2 \alpha)(1 + x^2 + r^2 - 2r\cos\alpha)^{1/2}} \qquad m \text{ (integer)} = 0 \ldots\ldots\ldots 8$$

Evaluation of C_m

Taking $m = 6$

$$C_6 = \int_{-\pi}^{\pi} \frac{\cos^6 \alpha \, d\alpha}{(1 + x^2 + r^2 - 2r\cos\alpha)^{1/2}} = \frac{4}{(1 + x^2 + r^2)^{1/2}} \int_0^{\pi/2} \frac{\cos^6 \alpha \, d\alpha}{(1 - k^2 \cos\alpha)^{1/2}}$$

With the successive transformations $\alpha = 2\phi + \pi$ and $\sin\phi = x$, the above integral takes the form:

$$C_6 = \frac{-4}{(1 + x^2 + r^2)^{1/2}(1 + k^2)^{1/2}} \int_0^{\pi/2} \frac{(1 - 2\sin^2\phi)^6 d\phi}{(1 - k'^2 \sin^2\phi)^{1/2}} = -\lambda \int_0^1 \frac{(1 - 2x^2)^6 dx}{\sqrt{(1 - x^2)(1 - k'^2 x^2)}} =$$

$$= -\lambda \left\{ A_0 - 12\, A_2 + 60 A_4 - 160 A_6 + 240 A_8 - 192 A_{10} + 64 A_{12} \right\}$$

where all A's can be determined by the recurrence formula of eq. (14) and $\lambda = + \dfrac{4}{(1 + x^2 + r^2)^{1/2}(1 + k^2)^{1/2}}$

Similarly

$$C_4 = -\lambda (A_0 - 8A_2 + 24\, A_4 - 32 A_6 + 16\, A_8)$$

$$C_2 = -\lambda (A_0 - 4A_2 + 4\, A_4)$$

and $C_0 = -\lambda\, A_0$

In general

$$C_n = (-1)^{n+1}\lambda\left\{A_o + \frac{(-2)n}{1!}A_2 + \frac{(-2)^2}{2!}n(n-1)A_4 + \frac{(-2)^3}{3!}n(n-1)(n-2)A_6 + \dots\right\}$$

Evaluation of D_m

In Reference 2 it is shown that when m is an odd integer $D_m = 0$.

In the case m = even, if $m = 2$, then

$$D_2 = \int_{-\pi}^{\pi}\frac{\cos^2\alpha d\alpha}{x^2+r^2\sin^2\alpha} = 4\int_0^{\pi/2}\frac{\cos^2\alpha d\alpha}{x^2+r^2\sin^2\alpha} = 4\left\{\int_0^{\pi/2}\frac{d\alpha}{x^2+r^2\sin^2\alpha} - \int_0^{\pi/2}\frac{\sin^2\alpha d\alpha}{x^2+r^2\sin^2\alpha}\right\}$$

$$= 4\left\{\int_0^{\pi/2}\frac{d\alpha}{x^2+r^2\sin^2\alpha} - \frac{1}{r^2}\int_0^{\pi/2}\left(1-\frac{x^2}{x^2+r^2\sin^2\alpha}\right)d\alpha\right\}$$

$$= 4\int_0^{\pi/2}\frac{d\alpha}{x^2+r^2\sin^2\alpha} - \frac{4}{r^2}\int_0^{\pi/2}d\alpha + \frac{4x^2}{r^2}\int_0^{\pi/2}\frac{d\alpha}{x^2+r^2\sin^2\alpha}$$

$$= 4\left(1+\frac{x^2}{r^2}\right)\int_0^{\pi/2}\frac{d\alpha}{x^2+r^2\sin^2\alpha} - \frac{4}{r^2}\int_0^{\pi/2}d\alpha$$

$$= \frac{2\pi}{r^2}\left\{\frac{(x^2+r^2)^{1/2}}{x} - 1\right\}$$

provided that $x \neq 0$.

Similarly

$$D_4 = 2\pi\left\{\frac{(r^2+x^2)^{3/2}}{xr^4} - \frac{r^2+x^2}{r^4} - \frac{1}{2r^2}\right\}$$

$$D_6 = 2\pi\left\{\frac{(r^2+x^2)^{5/2}}{xr^6} - \frac{(r^2+x^2)^2}{r^6} - \frac{(r^2+x^2)^2}{2r^4} - \frac{3}{8r^2}\right\}$$

In general

$$D_m = \frac{r^2+x^2}{r^2}\int_{-\pi}^{\pi}\frac{\cos^{m-2}\alpha\,d\alpha}{x^2+r^2} - \frac{1}{r^2}\int_{-\pi}^{\pi}\cos^{m-2}\alpha\,d\alpha$$

$$= \frac{r^2+x^2}{r^2}D_{m-2} + \frac{m-3}{m-2}\,(\text{last term of } D_{m-2})$$

Evaluation of E_m

The E_m integral will be shown to be a sum of all three kinds of complete elliptic integrals. The technique of transforming this integral into the complete elliptic integrals is given in Reference 2.

If $m = 6$, then

$$E_6 = \int_{-\pi}^{\pi}\frac{\cos^6\alpha\,d\alpha}{(x^2+r^2\sin^2\alpha)(1+x^2+r^2-2r\cos\alpha)^{1/2}} = \frac{2}{(1+x^2+r^2)^{1/2}x^2}\int_0^{\pi}\frac{\cos^6\alpha\,d\alpha}{(1+n\sin^2\alpha)(1-k^2\cos\alpha)^{1/2}}$$

where $n = \frac{r^2}{x^2}$ and $k^2 = \frac{2r}{1+x^2+r^2}$

With the successive transformations

$$\alpha = 2\phi+\pi \quad \text{and then} \quad \sin\phi = x$$

E_6 takes the form

$$E_6 = c\int_0^1 \frac{(1-2x^2)^6\,dx}{[1+4nx^2(1-x^2)]\sqrt{(1-x^2)(1-k'^2x^2)}}$$

where $c = \frac{4}{(1+x^2+r^2)^{1/2}x^2(1+k^2)^{1/2}}$, $k'^2 = \frac{k^2}{1+k^2}$

This can be reduced to

$$E_6 = c\left\{ I_a - 12I_b + 60I_c - 160\ I_d + 240\ I_e - 192\ I_f + 64\ I_g \right\}$$

where $$I_a = \int_o^1 \frac{dx}{[1+4n\ x^2(1-x^2)]\sqrt{(1-x^2)1-k'x^2}}$$

$$I_b = \int_o^1 \frac{x^2dx}{[1+4nx^2(1-x^2)]\sqrt{(1-x^2)(1-k'^2x^2)}}$$

$$I_c = \int_o^1 \frac{x^4dx}{[1+4nx^2(1-x^2)]\sqrt{(1-x^2)(1-k'^2x^2)}} \qquad \text{etc.}$$

In general it can be shown that

$$E_m = (-1)^m c\left\{ I_a + \frac{(-2)^1}{1!}\, m\ I_b + \frac{(-2)^2}{2!}\, m(m-1)\ I_c + \frac{(-1)^3}{3!}\, m(m-1)(m-2)\ I_d + \ldots\ldots \right\}$$

In Reference 10, by the same general procedure, the various I's were evaluated in terms of I_a, I_b and various A's . They are tabulated below.

If $\Delta = [1+4nx^2(1+x^2)]\sqrt{(1-x^2)(1-k'^2x^2)}$

then

$$I_c = \int_o^1 \frac{x^4dx}{\Delta} = -\frac{1}{4n}\, A_o + I_b + \frac{1}{4n}\ I_a$$

$$I_d = \int_o^1 \frac{x^6dx}{\Delta} = -\frac{1}{4n}\, A_2 - \frac{1}{4n}\, A_o + (\frac{1}{4n} + 1)I_b + \frac{1}{4n}\ I_a$$

$$I_e = \int_o^1 \frac{x^8dx}{\Delta} = -\frac{1}{4n}\, A_4 - \frac{1}{4n}A_2 - \frac{1}{4n}(1+\frac{1}{4n})A_o + (1+\frac{2}{4n})I_b + \frac{1}{4n}(1+\frac{1}{4n})I_a$$

$$I_f = \int_0^1 \frac{x^{10}dx}{\Delta} = -\frac{1}{4n}A_6 - \frac{1}{4n}A_4 - \frac{1}{4n}(1+\frac{1}{4n})A_2 - \frac{1}{4n}(1+\frac{2}{4n})A_o +$$

$$[\frac{1}{4n}(1+\frac{1}{4n}) + (1+\frac{2}{4n})]\ I_b + \frac{1}{4n}(1+\frac{2}{4n})I_a$$

$$I_g = \int_0^1 \frac{x^{12}dx}{\Delta} = -\frac{1}{4n}A_8 - \frac{1}{4n}A_6 - \frac{1}{4n}(1+\frac{1}{4n})A_4 - \frac{1}{4n}(1+\frac{2}{4n})A_2 -$$

$$-\frac{1}{4n}[\frac{1}{4n}(1+\frac{1}{4n})+(1+\frac{2}{4n})]A_o + [\frac{1}{4n}(1+\frac{2}{4n})+\frac{1}{4n}(1+\frac{1}{4n})+(1+\frac{2}{4n})]\ I_b$$

$$+\frac{1}{4n}[\frac{1}{4n}(1+\frac{1}{4n})+(1+\frac{2}{4n})]\ I_a$$

$$I_h = \int_0^1 \frac{x^{14}dx}{\Delta} = -\frac{1}{4n}A_{10} - \frac{1}{4n}A_8 - \frac{1}{4n}(1+\frac{1}{4n})A_6 - \frac{1}{4n}(1+\frac{2}{4n})A_4 -$$

$$-\frac{1}{4n}[\frac{1}{4n}(1+\frac{1}{4n})+(1+\frac{2}{4n})]\ A_2 - \frac{1}{4n}[\frac{1}{4n}(1+\frac{2}{4n})+\frac{1}{4n}(1+\frac{1}{4n})+(1+\frac{2}{4n})]\ A_o$$

$$+\left\{\frac{1}{4n}[\frac{1}{4n}(1+\frac{1}{4n})+(1+\frac{2}{4n})]+[\frac{1}{4n}(1+\frac{1}{4n})+\frac{1}{4n}(1+\frac{2}{4n})+(1+\frac{2}{4n})]\right\}\ I_b$$

$$+\frac{1}{4n}[\frac{1}{4n}(1+\frac{2}{4n})+\frac{1}{4n}(1+\frac{1}{4n})+(1+\frac{2}{4n})]\ I_a$$

$$I_k = \int_0^1 \frac{x^{16}dx}{\Delta} = -\frac{1}{4n}A_{12} - \frac{1}{4n}A_{10} - \frac{1}{4n}(1+\frac{1}{4n})A_8 - \frac{1}{4n}(1+\frac{2}{4n})A_6$$

$$-\frac{1}{4n}[(1+\frac{2}{4n})+\frac{1}{4n}(1+\frac{1}{4n})]\ A_4 - \frac{1}{4n}[\frac{1}{4n}(1+\frac{2}{4n})+\frac{1}{4n}(1+\frac{1}{4n})+(1+\frac{2}{4n})]\ A_2$$

$$-\frac{1}{4n}\left\{\frac{1}{4n}[(1+\frac{2}{4n})+\frac{1}{4n}(1+\frac{1}{4n})]+(1+\frac{2}{4n})+\frac{1}{4n}(1+\frac{1}{4n})+\frac{1}{4n}(1+\frac{2}{4n})\right\}\ A_o$$

$$+\left\{\frac{1}{4n}\left[\frac{1}{4n}\left(1+\frac{1}{4n}\right)+\left(1+\frac{2}{4n}\right)\right]+\left[\frac{1}{4n}\left(1+\frac{1}{4n}\right)+\frac{1}{4n}\left(1+\frac{2}{4n}\right)+\left(1+\frac{2}{4n}\right)\right]\right.$$

$$\left.+\frac{1}{4n}\left[\left(1+\frac{2}{4n}\right)+\frac{1}{4n}\left(1+\frac{1}{4n}\right)+\frac{1}{4n}\left(1+\frac{2}{4n}\right)\right]\right\} I_b$$

$$+\frac{1}{4n}\left\{\left[\frac{1}{4n}\left(1+\frac{1}{4n}\right)+\frac{1}{4n}\left(1+\frac{2}{4n}\right)+\left(1+\frac{2}{4n}\right)+\frac{1}{4n}\left[\left(1+\frac{2}{4n}\right)+\frac{1}{4n}\left(1+\frac{1}{4n}\right)\right]I_a\right\}.$$

where I_a , I_b are given in eq. (14) and A's by the recurrence formula (see eq. 14). The results have been written in rather extended form, in order to show the structure of the different expressions so that general rules may be set down for the recapture of an expression from the preceding one.

The following generalities can be deduced for the above expressions:

1. The coefficient of I_a is equal to $\frac{1}{4n}$ of the coefficient of I_b of the preceding expansion.
2. The coefficient of I_b is equal to the sum of the coefficients of I_a and I_b of the preceding expansion.
3. The coefficient of A_o is equal to $(-\frac{1}{4n})$ of the coefficient of I_b of the preceding expansion.
4. The coefficient of A_2 is equal to the coefficient of A_o of the preceding expansion, similarly that of A_4 is equivalent to the coefficient of A_2 of the preceding expansion, that of A_6 to that of the A_4 preceding, etc.
5. The highest subscript of A in a given expansion is four less than the exponent of the original integral i.e. (n-4) so that the A terms are from A_o to A_{n-4} .

With these general rules the result of any integration of the form I_n can be written in terms of the coefficients of the previous expansion I_{n-2} .

After the three types of integral C_m, D_m, and E_m which are encountered

in the evaluation of the second blade harmonic of eq. (C-1) have been determined, then by a trivial algebraic manipulation the final result is obtained in the form of eq. (15) and (16).

APPENDIX D

by W. Jacobs

This appendix describes the use of the two-dimensional mathematical model of the counterrotating propeller configuration in order to obtain the pressure signals due to the independent motion of each of the two cascades of blades representing the propellers.

The coordinate axes are as in Sketch 2.

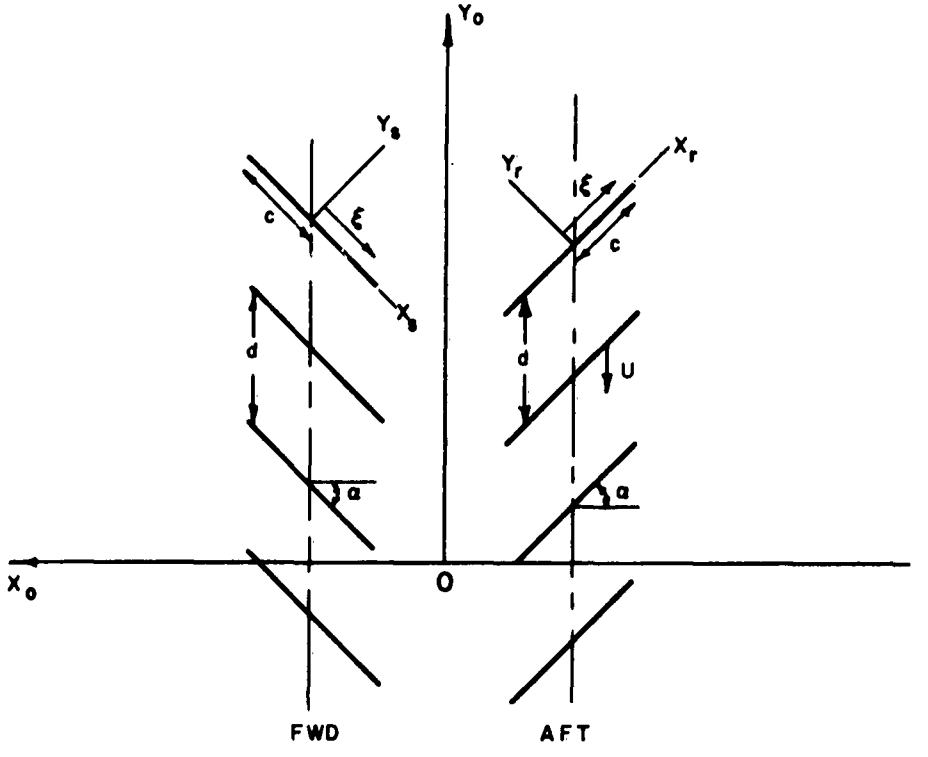

If the field point (x,y) is referred to the axes in a blade of an infinite cascade, then its velocity potential, referred to the singularities (ξ,0) on the blade, is given by

$$\phi(x,y) = \sum_{n=-\infty}^{\infty} \int_{-c}^{c} \frac{\gamma}{2\pi} \tan^{-1} \frac{[y - (\eta \pm nd)\cos\alpha]}{[x - (\eta \pm nd)\sin\alpha - \xi]} \, d\xi \qquad (D\text{-}1)$$

where γ = the strength of the circulation

$\eta = Ut$

U = rotational speed of the propeller, ft/sec.

n = the blade number in the infinite cascade and the other symbols are as defined before.

For a flat-plate distribution of the circulation

$$\gamma = \frac{{}_o\Gamma}{c\pi}\sqrt{\frac{c-\xi}{c+\xi}} \tag{D-2}$$

The vertical velocity is then

$$v = \frac{\partial \phi}{\partial y} = \frac{-{}_o\Gamma}{2\pi^2 c} \sum_{n=\infty}^{\infty} \int_{-c}^{c} \sqrt{\frac{c-\xi}{c+\xi}} \frac{[x-(\eta \pm nd)\sin\alpha - \xi]d\xi}{[x-(\eta \pm nd)\sin\alpha - \xi]^2 + [y-(\eta \pm nd)\cos\alpha]^2}$$

or

$$v = \frac{-{}_o\Gamma}{2\pi^2 c} \mathrm{Re} \sum_{n=-\infty}^{\infty} \int_{-c}^{c} \sqrt{\frac{c-\xi}{c+\xi}} \frac{d\xi}{(x-\xi) \mp i(y-\eta e^{-i\alpha} \mp nde^{-i\alpha})} \tag{D-3}$$

Since $(x-\xi) \mp i(y-\eta e^{-i\alpha} \mp nde^{-i\alpha}) =$

$$\frac{de^{-i\alpha}}{\pi}\left\{\frac{\pi e^{i\alpha}}{d}\left[x - \xi \mp i(y-\eta e^{-i\alpha})\right] \pm in\pi\right\}$$

$$v = -\frac{-{}_o\Gamma}{2\pi cd} \mathrm{Re}\left\{e^{i\alpha} \sum_{n=-\infty}^{\infty} \int_{-c}^{c} \sqrt{\frac{c-\xi}{c+\xi}} \frac{d\xi}{\frac{\pi e^{i\alpha}}{d}\left\{x-\xi \mp i(y-\eta e^{-i\alpha})\right\} \pm in\pi}\right\} \tag{D-4}$$

But $\sum_{n=-\infty}^{\infty} \frac{1}{z-in\pi} = \coth z$

and $\coth z = 1 + 2\sum_{m} e^{-2mz}$ provided that

$R(z) > 0$, i.e. $\frac{\pi}{d}[(x-\xi)\cos\alpha \pm y\sin\alpha] > 0$

There are two possibilities:

1) $(x-\xi)\cos\alpha \pm y \sin\alpha > 0$

in which case the time-dependent part of eq. (D-4) becomes

$$v = \frac{-o\Gamma}{\pi cd} \mathrm{Re}\left\{ e^{i\alpha} \sum_m \int_{-c}^{c} \sqrt{\frac{c-\xi}{c+\xi}} \exp\left[-2\pi \frac{me^{i\alpha}}{d}(x-\xi \mp iy \pm i\eta e^{-i\alpha})\right] d\xi \right.$$

or

$$v = \frac{-o\Gamma}{\pi cd} \mathrm{Re} \sum_m \left\{ e^{i\alpha} e^{\frac{-2\pi me^{i\alpha}x}{d}} e^{\mp \frac{i2\pi me^{i\alpha}y}{d}} e^{\mp \frac{i2\pi m\eta}{d}} \int_{-c}^{c} \sqrt{\frac{c-\xi}{c+\xi}}\, e^{\frac{2\pi me^{i\alpha}\xi}{d}}\, d\xi \right\}$$

Let $\xi = c\cos\theta$, then $d\xi = -c\sin\theta d\theta$ and when $\xi = -c$, $\theta = \pi$ and $\xi = +c$, $\theta = 0$. Then

$$\int_{-c}^{c} \sqrt{\frac{c-\xi}{c+\xi}}\, e^{\frac{2\pi me^{i\alpha}\xi}{d}} d\xi = c\int_{o}^{\pi} (1-\cos\theta) e^{\frac{2\pi me^{i\alpha}c}{d}\cos\theta} d\theta$$

$$= c\pi\left\{ I_b\left(\frac{2\pi mce^{i\alpha}}{d}\right) - I_1\left(\frac{2\pi mce^{i\alpha}}{d}\right) \right\}$$

and

$$v = \frac{-o\Gamma}{d} \mathrm{Re} \sum_m \left\{ e^{i\alpha} e^{\frac{-2\pi me^{i\alpha}x}{d}} e^{\mp \frac{i2\pi me^{i\alpha}y}{d}} e^{\mp \frac{i2\pi m\eta}{d}} \left[I_o(\lambda) - I_1(\lambda) \right] \right\}$$

$$\text{where} \quad \lambda = \frac{2\pi mce^{i\alpha}}{d} \tag{D-5}$$

The velocity distribution along the blade chord will be obtained by setting $y=0$, $x = c\cos\theta$. Then

$$v(x,\theta) = -\frac{\Gamma_o}{d}\,\mathrm{Re}\sum_m \left\{ e^{i\alpha}\, e^{\mp imvt} \exp\left(-\frac{2\pi m e^{i\alpha} c\cos\theta}{d}\right)[I_o(\lambda) - I_1(\lambda)] \right\}$$

or

$$v(x,\theta) = -\frac{\Gamma_o}{d}\,\mathrm{Re}\sum_m \left\{ e^{i\alpha}\, e^{\mp imvt} [I_o(\lambda)-I_1(\lambda)][J_o(\mu)+2\sum_{n=1}^{\infty}(-i)^n J_n(\mu)\cos n\theta] \right\}$$

$$\text{where}\quad \mu = \frac{2\pi mc}{d}\, e^{-i\left(\frac{\pi}{2}-\alpha\right)} \qquad \text{(D-6)}$$

$$\nu = 2\pi U/d$$

By using the acceleration potential, the pressure can be obtained as before, at any point defined by the field point function $(\sin\theta_1)/r_1$. The dimensionless pressure signal due to the velocity distribution (6) is

$$\frac{P}{T'} = \frac{4\pi V_R}{m_B \Omega d}\left(\frac{\sin\theta_1}{r_1}\right)\mathrm{Re}\sum_m \left\{ e^{i\alpha}\, e^{\mp imvt} [I_o(\lambda)-I_1(\lambda)]\left\{C(\mu)\left[J_o(\mu)-iJ_1(\mu)\right]+iJ_1(\mu)\right\}\right\} \qquad \text{(D-7)}$$

where m_B = number of blades in the propeller

Ω = 2π(r.p.s.)

V_R = resultant velocity along the blade chord

$T' = \dfrac{T}{\pi b^2} = \dfrac{m\rho\Omega_o\Gamma}{2\pi}$

and all geometric characteristics are measured at 0.7 propeller radius.

2) $(\xi - x)\cos\alpha \mp y\sin\alpha > 0$ in which case the time-dependent part of eq. (4) becomes

$$v = \frac{\Gamma_o}{\pi cd}\,\mathrm{Re}\sum_m \left\{ e^{i\alpha}\, e^{\frac{2\pi m e^{i\alpha} x}{d}}\, e^{\mp\frac{i2\pi m e^{i\alpha} y}{d}}\, e^{\mp\frac{i2\pi m\eta}{d}} \int_{-c}^{c} \sqrt{\frac{c-\xi}{c+\xi}}\, e^{-\frac{2\pi m e^{i\alpha}\xi}{d}}\, d\xi \right\}$$

Let $\xi = -c\cos\theta$, then $d\xi = c\sin\theta d\theta$ and when $\xi = -c$, $\theta=0$ and $\xi = +c$, $\theta=\pi$. Then

$$\int_{-c}^{c}\sqrt{\frac{c-\xi}{c+\xi}}\, e^{\frac{-2\pi m e^{i\alpha}\xi}{d}}\, d\xi = c\int_{o}^{\pi}(1+\cos\theta)\, e^{\frac{2\pi m e^{i\alpha} c\cos\theta}{d}}\, d\theta$$

$$= c\pi\left\{ I_o\left(\frac{2\pi mce^{i\alpha}}{d}\right) + I_1\left(\frac{2\pi mce^{i\alpha}}{d}\right)\right\}$$

The velocity distribution along the blade chord will be obtained by setting $y = 0$, $x = -c\cos\theta$. Then

$$v(x,\theta) = \frac{\Gamma_o}{d}\, \mathrm{Re}\sum_m \left\{ e^{i\alpha}\, e^{\pm im\nu t}\, \exp\left(-\frac{2\pi m e^{i\alpha} c\cos\theta}{d}\right)[I_o(\lambda)+I_1(\lambda)]\right\}$$

or

$$v(x,\theta) = \frac{\Gamma_o}{d}\mathrm{Re}\sum_m \left\{ e^{i\alpha}\, e^{\pm im\nu t}\, [I_o(\lambda)+I_1(\lambda)][J_o(\mu)+2\sum_{n=1}^{\infty}(-i)^n J_n(\mu)\cos n\theta]\right\}$$

(D-8)

and

$$\frac{P}{\Gamma} = -\frac{4\pi V_R}{m_B \Omega d}\left(\frac{\sin\theta_1}{r_1}\right)\mathrm{Re}\sum_m \left\{ e^{i\alpha}\, e^{\pm im\nu t}\, [I_o(\lambda)+I_1(\lambda)]\left\{ C(\mu)\left[J_o(\mu)-iJ_1(\mu)\right]+iJ_1(\mu)\right\}\right\}$$

(D-9)

Whether equation (D-7) or equation (D-9) is used to calculate the pressure signal at a point x,y referred to particular blade-chord axes depends on the condition

1) $(x-c\cos\theta)\cos\alpha \pm y\sin\alpha > 0$

or

2) $(-c\cos\theta - x)\cos\alpha \mp y\sin\alpha > 0$

at that point. It is found that, for the case of blade chord centered on the x_o-axis and for points on the ship's centerplane at $r/b = 1.2$ and x_o/b from 0 to 8, eq. (D-7) applies to the after propeller and eq. (D-9) to the forward propeller.

INITIAL DISTRIBUTION LIST

Copies		
50	Commanding Officer and Director David Taylor Model Basin Washington 7, D. C. Attention: Code 513	
9	Chief Bureau of Ships Department of the Navy Washington 25, D. C. Attention: Technical Information Bureau (Code 335)	(3)
	Ship Design (Code 410)	(1)
	Ship Silencing Branch (Code 345)	(1)
	Preliminary Design (Code 420)	(2)
	Hull Design (Code 440)	(1)
	Scientific and Research (Code 442)	(1)
2	Director Ordnance Research Laboratory Pennsylvania State University P. O. Box 30 University Park, Pennsylvania	
1	Mr. Hollinshead De Luce Bethlehem Steel Company Shipbuilding Division Central Technical Division Quincy 69, Massachusetts	
2	Gibbs and Cox, Inc. 21 West Street New York 6, New York Attention: Mr. W. F. Gibbs Mr. W. Bachman	
1	Reed Research Inc. 1048 Potomac Street, N. W. Washington 7, D. C. Attention: Mr. S. Reed	
1	Dr. A. G. Strandhagen, Head Department of Engineering Mechanics University of Notre Dame Notre Dame, Indiana	
2	Department of Naval Architecture and Marine Engineering Massachusetts Institute of Technology Cambridge 39, Massachusetts	

Copies	
2	Dr. H. W. Lerbs, Director Hamburgische Schiffbau Versuchsanstalt Bramfelder Strasse 164 Hamburg 33, Germany
1	Capt. E. S. Arentzen, USN Commanding Officer U. S. Naval Reserve Officers Training Corps Massachusetts Institute of Technology Cambridge 39, Massachusetts
1	Dr. J. V. Wehausen Department of Engineering Institute of Engineering Research University of California Berkeley 4, California
1	Dr. J. Lunde, Director Skipsmodelltanken Norges Tekniske Hogskole Trondheim, Norway
1	Librarian Society of Naval Architects and Marine Engineers 74 Trinity Place New York, New York
1	Professor R. B. Couch, Chairman Department of Naval Architecture and Marine Engineering University of Michigan Ann Arbor, Michigan
1	Mr. Sam Elhai Propulsion Division (P8063) U. S. Naval Ordnance Test Station 125 S. Grand Avenue Pasadena, California
2	Administrator Webb Institute of Naval Architecture Glen Cove, New York Attention: Post Graduate School for Officers

Copies

1 Mr. John Kane
Engineering Technical Department
Newport News Shipbuilding and
Dry Dock Company
Newport News, Virginia

1 Mr. V. L. Russo, Deputy Chief
Officer of Ship Construction
Maritime Administration
Washington 25, D. C.

1 Mr. Caesar Tangerini, Head
Main Propulsion Section
Engineering Specification Branch
Maritime Administration
Washington 25, D. C.

1 Dr. G. Weinblum
Universitaet Hamburg
Berliner Tor 21, Z620
Hamburg 1, Germany

1 Dr. Ir. J. D. Van Manen
Ned. Scheepsbouwkundig Proefstation
Wageningen
Haagsteer 2, The Netherlands

1 Editor
Applied Mechanics Review
Southwest Research Institute
8500 Culebra Road
San Antonio 6, Texas

2 Sr. M. Acevedo, Director
Canal De Experiencias Hidrodinamicas
El Pardo (Madrid), Spain

5 Chief of Naval Research
Department of the Navy
Washington 25, D. C.
For Distribution to:
Code 438 (4)
Code 466 (1)

1 Director
U. S. Naval Research Laboratory
(Code 2000)
Washington 25, D. C.

Copies

3 Commander
U. S. Naval Ordnance Test Station
Pasadena Annex
3202 East Foothill Boulevard
Pasadena, California
For Additional Distribution to:
Technical Library (1)
Head, Thrust Producer Section (1)

1 Commanding Officer
Office of Naval Research
Branch Office
346 Broadway
New York 13, New York

1 Commanding Officer
Office of Naval Research
Branch Office
1000 Geary Street
San Francisco 9, California

1 Commanding Officer
Office of Naval Research
Branch Office
Navy 100, F. P. O.
New York, New York

1 Dr. L. G. Straub, Director
St. Anthony Falls Laboratory
University of Minnesota
Minneapolis, Minnesota

10 Commander
Armed Services Technical Informati
Agency
Attention: TIPDR
Arlington Hall Station
Arlington 12, Virginia

1 Mr. C. W. Prohaska
Direktor, Hydro-og
Aerodynamisk Laboratorium
Hjorlekservej 99
Lyngby, Denmark

2 National Physical Laboratory
Teddington, Middlesex
England
Attention: Dr. A. Silverleaf
Dr. F. H. Todd

Copies

1 Chief
Bureau of Weapons
Department of the Navy
Washington 25, D. C.

2 Commander
U. S. Naval Ordnance Laboratory
White Oak
Silver Spring, Maryland
Attention: Library

1 Commanding Officer
Office of Naval Research
Branch Office
495 Sumner Street
Boston 10, Massachusetts

1 Commanding Officer
Office of Naval Research
Branch Office
The John Crerar Library Building
10th Floor
86 East Randolph Street
Chicago 1, Illinois

1 Commanding Officer
Office of Naval Research
Branch Office
1030 East Green Street
Pasadena 1, California

1 Director
Hydrodynamics Laboratory
California Institute of Technology
Pasadena 4, California

1 Professor H. A. Schade, Director
Institute of Engineering Research
University of California
Berkeley 4, California

1 Editor
Engineering Index, Inc.
29 West 39th Street
New York, New York

Copies

1 Librarian
Institute of Aerospace Sciences, I
2 East 64th Street
New York 21, New York

1 Director
Paris Towing Tank
6, Boulevard Victor
Paris XV, France

1 Director of the "Instituto
Nazionale per Studi Esperiense d
Architettura Navale"
Via Ventiquattro Maggio, 11
Roma, Italy